# Identification of Structural and Functional *O*-Linked *N*-Acetylglucosamine-bearing Proteins in *Xenopus laevis* Oocyte*

Vanessa Dehennaut‡§¶, Marie-Christine Slomianny‡‖, Adeline Page‖**, Anne-Sophie Vercoutter-Edouart‡, Catherine Jessus‡‡, Jean-Claude Michalski‡, Jean-Pierre Vilain§, Jean-François Bodart§, and Tony Lefebvre‡§§

***O*-Linked *N*-acetylglucosaminylation (*O*-GlcNAcylation) (or *O*-linked *N*-acetylglucosamine (*O*-GlcNAc)) is an abundant and reversible glycosylation type found within the cytosolic and the nuclear compartments. We have described previously the sudden *O*-GlcNAcylation increase occurring during the *Xenopus laevis* oocyte $G_2$/M transition, and we have demonstrated that the inhibition of *O*-GlcNAc-transferase (OGT) blocked this process, showing that the *O*-GlcNAcylation dynamism interferes with the cell cycle progression. In this work, we identified proteins that are *O*-GlcNAc-modified during the $G_2$/M transition. Because of a low expression of *O*-GlcNAcylation in *Xenopus* oocyte, classical enrichment of *O*-GlcNAc-bearing proteins using *O*-GlcNAc-directed antibodies or wheat germ agglutinin lectin affinity were hard to apply, albeit these techniques allowed the identification of actin and erk2. Therefore, another strategy based on an *in vitro* enzymatic labeling of *O*-GlcNAc residues with azido-GalNAc followed by a chemical addition of a biotin alkyne probe and by enrichment of the tagged proteins on avidin beads was used. Bound proteins were analyzed by nano-LC-nano-ESI-MS/MS allowing for the identification of an average of 20 *X. laevis* oocyte *O*-GlcNAcylated proteins. In addition to actin and $\beta$-tubulin, we identified metabolic/functional proteins such as PP2A, proliferating cell nuclear antigen, transitional endoplasmic reticulum ATPase, aldolase, lactate dehydrogenase, and ribosomal proteins. This labeling allowed for the mapping of a major *O*-GlcNAcylation site within the 318–324 region of $\beta$-actin. Furthermore immunofluorescence microscopy enabled the direct visualization of *O*-GlcNAcylation and OGT on the meiotic spindle as well as the observation that chromosomally bound proteins were enriched in *O*-GlcNAc and OGT. The biological relevance of this post-translational modification both on microtubules and on chromosomes remains to be determined. However, the mapping of the *O*-GlcNAcylation sites will help to underline the function of this post-translational modification on each identified protein and will provide a better understanding of *O*-GlcNAcylation in the control of the cell cycle. *Molecular & Cellular Proteomics 7:2229–2245, 2008.***

Cells divide according to a spatially and a temporally regulated process called the cell cycle. This intricate mechanism is usually divided into four phases, namely $G_1$ (Gap1), S (DNA replication), $G_2$ (Gap2), and M (mitosis/meiosis). To ensure successful completion of its division, each phase and each checkpoint ($G_0$/$G_1$, $G_1$/S, $G_2$/M, and metaphase/anaphase) are tightly controlled by several factors that work in concert. Cyclin-dependent kinases (cdks)[1] and their specific regulators cyclins are the best described regulators monitoring the cell cycle progression. A dysregulation of these cdks leads to an uncontrolled cell division ending up in tissue cancerization (for a review, see Ref. 1).

*Xenopus laevis* oocyte has been widely used as a model for studying the regulation of the cell cycle. The imposing size of this cell (1.3-mm diameter with a nucleus of 300 $\mu$m), a total protein quantity of 25 $\mu$g/oocyte, and its amenability for manipulation made this model powerful for the characterization and the identification of many key cell cycle components, such as the M phase-promoting factor (MPF) and the cytostatic factor (2, 3). During oogenesis, the oocyte accumulates nutrients and materials (mRNAs and enzymes) that will be

[1] The abbreviations used are: cdk, cyclin-dependent kinase; erk, extracellular signal-regulated kinase; MAPK, mitogen-activated protein kinase; MPF, M-phase promoting factor; *O*-GlcNAcylation, *O*-linked *N*-acetylglucosaminylation; PTM, post-translational modification; GalNAz, azido-GalNAc; UDP-GalNAz, uridine diphosphoazido-*N*-acetylgalactosamine; MSDB, Mass Spectrometry Protein Sequence Database; OGT, *O*-GlcNAc-transferase; PCNA, proliferating cell nuclear antigen; TER, transitional endoplasmic reticulum; LH, luteinizing hormone; PUGNAc, *O*-(2-acetamido-2-deoxy-D-glucopyranosylidene)-amino-*N*-phenylcarbamate; IB, immunoprecipitation buffer; HRP, horseradish peroxidase; GalT1, $\beta$1,4-galactosyltransferase I; GAPDH, glyceraldehyde-3-phosphate dehydrogenase; eIF, eukaryotic initiation factor.

From the ‡UMR-CNRS 8576, Unité de Glycobiologie Structurale et Fonctionnelle, §EA 4020, Laboratoire de Régulation des Signaux de Division, and **Centre Commun de Mesures de Spectrométrie de Masse, Université des Sciences et Technologies de Lille, IFR 147, 59655 Villeneuve d'Ascq, France and ‡‡UMR-CNRS 7622, Laboratoire de Biologie du Développement, Equipe Biologie de l'Ovocyte, Université Pierre et Marie Curie, 75252 Paris, France

Received, October 11, 2007, and in revised form, June 24, 2008
Published, MCP Papers in Press, July 9, 2008, DOI 10.1074/mcp.M700494-MCP200

necessary to carry out meiosis and for the further fertilization and embryogenesis. At the end of oogenesis, the oocyte is physiologically blocked in prophase of the first meiotic division in a $G_2$-like stage and is called immature oocyte. After progesterone stimulation (produced and secreted by follicular cells surrounding the oocyte in response to LH), the oocyte resumes meiosis in a $G_2$/M analogue transition phase; this process termed oocyte maturation is first accompanied by the germinal vesicle breakdown, the condensation of the chromosomes, and the spindle assembly (for a review, see Ref. 4). At the molecular level, the oocyte maturation is in part under the control of cdc25C and myt1, a dual specificity phosphatase and a dual specificity kinase, respectively, acting on cdk1 Thr-14 and Tyr-15. The phosphorylation status of both residues is critical for the activation of the MPF (cdk1-cyclin B) (5, 6). Concomitantly to the MPF, the mos-erk2 pathway, which is required for normal spindle formation (7), is also activated. At the end of maturation, the meiotic cell cycle is stopped in metaphase II in anticipation for fertilization.

We have shown recently that the *X. laevis* oocyte maturation was accompanied by an increase in *O*-GlcNAcylation (8) and that the inhibition of *O*-GlcNAc-transferase (OGT), the enzyme transferring the GlcNAc group to the target proteins, delayed or blocked this process (9) depending on the inhibitor concentration. *O*-GlcNAcylation is a particular PTM in that it possesses features different from other glycosylation types (for reviews, see Refs. 10–13). First, *O*-GlcNAcylation is the modification of serine and threonine residues by a single *N*-acetylglucosamine moiety that is neither elongated nor epimerized. Second, it is found within the cytosolic and the nuclear compartments, whereas the "classical" *N*- and *O*-glycosylation types are mainly confined into the lumen of organelles (endoplasmic reticulum, Golgi, and lysosome) and the secretory pathway, including membrane-bound proteins. Third, *O*-GlcNAcylation is highly dynamic like phosphorylation. These two PTMs can indeed compete at the same or a neighboring site. Although *O*-GlcNAcylation is abundantly widespread in eukaryotes and although more than 600 proteins bearing *O*-GlcNAc have been identified to date (for reviews, see Refs. 11–13), in most cases its exact function(s) remains to be elucidated. Nevertheless *O*-GlcNAcylation seems to be crucial for many cellular processes such as transcription, cell signaling, intracellular trafficking, development, and the cell cycle. Several studies support the functional importance of *O*-GlcNAcylation in the cell cycle progression (for a review, see Ref. 14). For instance, microinjection of bovine galactosyltransferase, an enzyme capping terminal GlcNAc residues, inhibited *Xenopus* oocyte M phase entry and blocked M to S phase transition (15). At the same time, Slawson *et al.* (16) showed that the perturbation of *Xenopus* oocyte *O*-GlcNAcylation levels either by glucosamine or PUGNAc treatment modified the maturation kinetics. Later PUGNAc was used to inhibit the *O*-GlcNAc-hydrolyzing enzyme *O*-*N*-acetylglucosaminidase in somatic cultured cells: PUGNAc-treated cells progressed more slowly through the cell cycle than the untreated cells (17). Therefore, it appears that *O*-GlcNAcylation, like many other PTMs, plays a determining role in the regulation of the cell cycle. For example, the impact of histone modifications by methylation, acetylation, and phosphorylation in the relaxation/condensation of chromatin during the $G_2$/M transition has been described intensively (for a review, see Ref. 18). The regulation of cyclin stability by ubiquitination and the regulation of MPF activity by phosphorylation are two other examples of the control of the cell cycle by PTMs. To better understand how *O*-GlcNAc levels can control the cell cycle, the identification of proteins for which *O*-GlcNAcylation content varies during this process appears to be essential. Because of a low *O*-GlcNAcylation expression in *Xenopus* oocyte in comparison with human somatic cells, the enrichment of *O*-GlcNAc-bearing proteins by classical approaches (based on immunoprecipitation or lectin affinity) was insufficient for the identification of *O*-GlcNAcylated proteins even if it previously allowed for the identification of *O*-GlcNAc-modified actin and erk2. Here we therefore opted for an *in vitro* modification of *O*-GlcNAc proteins with azido-GalNAc (GalNAz) followed by a chemical addition of a biotin probe. This strategy led to the identification of more than 20 proteins involved in cell architecture, metabolism, and protein translation and to the localization of an *O*-GlcNAcylated site within the 318–324 region of $\beta$-actin. Furthermore immunofluorescence microscopy studies showed that the meiotic spindle interacts with OGT, bears *O*-GlcNAc, and/or interacts with *O*-GlcNAcylated proteins and that condensed chromatin also interacts with OGT and is enriched in *O*-GlcNAcylated proteins. The latter observations further underline the importance of *O*-GlcNAcylation in cell division and in the progression of the cell cycle.

## EXPERIMENTAL PROCEDURES

### *Animals, Chemicals, and Bioreagents*

Adult *Xenopus* females came from the University of Rennes I (Rennes, France). Tricaine methane sulfonate was purchased from Sandoz (Levallois-Perret, France). Collagenase A and protease inhibitors were purchased from Roche Applied Science. Progesterone, agarose-coupled WGA beads, agarose-coupled avidin beads, peroxidase-labeled avidin, rabbit polyclonal anti-*O*-GlcNAc-transferase (DM17), and mouse monoclonal anti-$\beta$-tubulin (Tub2.1) were purchased from Sigma-Aldrich. Biotin alkyne, Click-it™ *O*-GlcNAc enzymatic labeling system, Alexa Fluor 488 goat anti-mouse IgG, Alexa Fluor 488 goat anti-rabbit IgG, and Alexa Fluor 594 goat anti-rabbit IgG were purchased from Molecular Probes/Invitrogen. Mouse monoclonal anti-*O*-GlcNAc (RL2) was purchased from Affinity Bioreagents (Golden, CO). CTD110.6 was a kind gift from Prof. Gerald W. Hart's group (Johns Hopkins University, Baltimore, MD). Mouse monoclonal anti-erk2 (D-2), rabbit polyclonal anti-actin (I-19), mouse monoclonal anti-$\alpha$-tubulin (B-5-1-2), and normal rabbit IgG control (sc-2027) were from Santa Cruz Biotechnology, Inc. (Santa Cruz, CA). The guinea pig polyclonal antibody directed against the 35-kDa catalytic subunit of PP2A was described previously (19). Mouse monoclonal anti-PCNA was purchased from Dako (Glostrup, Denmark). Anti-mouse (IgG or IgM), anti-rabbit (IgG), and anti-guinea pig horseradish peroxidase-

labeled secondary antibodies and enhanced chemiluminescence reagents were purchased from GE Healthcare. Texas Red-coupled anti-mouse IgM was from Jackson ImmunoResearch Europe Ltd. (Suffolk, UK).

### *Handling of Oocytes*

After anesthetizing *Xenopus* females by immersion in 1 g·liter$^{-1}$ MS222 solution (tricaine methane sulfonate), ovarian lobes were surgically removed and placed in ND96 medium (96 mM NaCl, 2 mM KCl, 1.8 mM $CaCl_2$, 1 mM $MgCl_2$, 5 mM HEPES-NaOH, pH 7.5). Fully grown stage VI oocytes were isolated, and follicle cells were partially removed by a collagenase treatment for 30 min (1 mg·ml$^{-1}$ collagenase A) followed by a manual microdissection. Oocytes were stored at 14 °C in ND96 medium until experiments.

### *Stimulation and Analysis of $G_2$/M Transition (Meiotic Resumption) in Xenopus Oocytes*

Meiotic resumption (M phase entry) was induced by incubating $G_2$-arrested oocytes in ND96 medium containing 10 $\mu$M progesterone. Progesterone is naturally synthesized and secreted by follicular cells (after stimulation by the hypophyseal gonadotropin LH) that are around the oocyte. Progesterone is then transformed into different metabolites that trigger meiotic resumption. Germinal vesicle breakdown achievement, a sign of M phase entry, was scored by the appearance of a white spot at the animal pole of the oocyte and checked by hemisection after heat fixation (3 min at 100 °C).

### *Immunoprecipitation Assays*

Batches of 20 immature and matured oocytes and around 8·10$^6$ HeLa cells were lysed in 1 ml of immunoprecipitation buffer (IB; 10 mM Tris/HCl, 150 mM NaCl, 1 mM EDTA, 1% (v/v) Triton X-100, 0.5% (w/v) sodium deoxycholate, 0.1% (w/v) SDS, protease inhibitors, pH 7.4). After centrifugation at 20,000 × *g*, supernatants were incubated overnight at 4 °C with either 10 $\mu$l of anti-*O*-GlcNAc (RL2), anti-actin antibodies, or control IgG. Then 50 $\mu$l of protein G (for RL2 immunoprecipitation) or protein A (for actin immunoprecipitations) were added to the samples that were newly placed for 1 h at 4 °C. Four washes were carried out in the following order: IB, IB supplemented with 0.5 M NaCl, IB/TNE (10 mM Tris/HCl, 150 mM NaCl, 1 mM EDTA, pH 7.4) (v/v), and finally TNE alone. Immunoprecipitates were resuspended in Laemmli buffer and boiled.

### *Enrichment of O-GlcNAc-bearing Proteins with WGA Immobilized on Agarose Beads*

These experiments were performed in two conditions as described previously (8, 20): in non-denaturing conditions that permitted the recovery of all *O*-GlcNAcylated proteins and their associated partners and in more stringent conditions in which all protein-protein interactions were broken.

*WGA Enrichment in Non-denaturing Conditions*—Batches of 20 immature or matured oocytes were removed and lysed in 100 $\mu$l of homogenization buffer (60 mM $\beta$-glycerophosphate, 15 mM *para*-nitrophenyl phosphate, 25 mM MOPS, 15 mM EGTA, 15 mM $MgCl_2$, 2 mM DTT, 1 mM sodium orthovanadate, 1 mM NaF, proteases inhibitors, pH 7.2). After centrifugation at 20,000 × *g*, supernatants were collected and diluted with PBS (145 mM NaCl, 10 mM $Na_2HPO_4$, 10 mM $NaH_2PO_4$, pH 7.4). Then samples were incubated for 90 min at 4 °C with 50 $\mu$l of WGA-agarose beads. The bound proteins were collected by centrifugation, and the beads were washed four times with PBS, resuspended in 50 $\mu$l of Laemmli buffer, and boiled for 10 min.

*WGA Enrichment in Stringent Conditions*—Batches of 20 immature or matured oocytes were removed and lysed in 200 $\mu$l of homogenization buffer (10 mM Tris/HCl, 1 mM EDTA, 1 mM EGTA, 0.5% (v/v) Triton X-100, proteases inhibitors, pH 7.5). After centrifugation at 20,000 × *g*, supernatants were collected, and 800 $\mu$l of homogenization buffer were added. Then samples were incubated with WGA-agarose beads, and WGA-bounds proteins were collected, washed four times with washing buffer (10 mM Tris/HCl, 100 mM NaCl, 0.4% (w/v) sodium deoxycholate, 0.3% (w/v) SDS, 0.2% (v/v) Nonidet P-40, pH 7.5), resuspended in Laemmli buffer, and boiled.

### *Labeling of O-GlcNAc-bearing Proteins by GalNAz and Biotin Alkyne Enrichment on Avidin Beads*

Batches of 10 immature or matured oocytes were lysed in 100 $\mu$l of homogenization buffer. 20 $\mu$g of bovine $\alpha$-crystallin were used as a positive control. Labeling of *O*-GlcNAc-bearing proteins by GalNAz and biotin alkyne was done using the Click-it *O*-GlcNAc enzymatic labeling system and the Click-it glycoprotein detection kit (biotin alkyne) according to the manufacturer's instructions. After labeling, the proteins were precipitated using the methanol/chloroform kit protocol and resuspended in 50 $\mu$l of Tris/HCl, pH 8.0, containing 0.1% (w/v) SDS. 700 $\mu$l of enrichment buffer (1% (v/v) Triton X-100, 0.1% (w/v) SDS in PBS) were added to the sample before incubating with 50 $\mu$l of avidin-coupled beads (1 h at 4 °C). The avidin-bound proteins were collected, washed three times with the enrichment buffer, resuspended in Laemmli buffer, and boiled. For the immunoprecipitation of erk2, methanol/chloroform-precipitated proteins were resuspended in immunoprecipitation buffer and treated as described above.

### *SDS-PAGE and Western Blotting*

Proteins (the equivalent of one oocyte was loaded per lane) were separated by 10% SDS-PAGE or by 17.5% modified SDS-PAGE (21, 22) for erk2 (this level of cross-linking allows a better discrimination between the active and the inactive forms of these proteins) and electroblotted onto nitrocellulose sheet. Although the quantity of proteins remains rather constant in the *Xenopus* oocyte, equal loading and transfer efficiency were checked using Ponceau red staining. Blots were saturated with 5% (w/v) nonfat milk in TBS-Tween (15 mM Tris, 140 mM NaCl, 0.05% (v/v) Tween) for 45 min or in 3% BSA in TBS-Tween for the avidin-HRP blotting. Primary antibodies were incubated overnight at 4 °C. Mouse monoclonal anti-*O*-GlcNAc (RL2), mouse monoclonal anti-erk2 (D-2), mouse monoclonal anti-$\alpha$-tubulin, mouse monoclonal anti-PCNA, guinea pig polyclonal anti-PP2A, and rabbit polyclonal anti-actin were used at a dilution of 1:1000. Mouse monoclonal anti-*O*-GlcNAc CTD110.6 was used at a dilution of 1:4000. Then membranes were washed three times for 10 min in TBS-Tween and incubated with either an anti-mouse (IgG or IgM) horseradish peroxidase-labeled secondary antibody or an anti-rabbit IgG or an anti-guinea pig IgG horseradish peroxidase-labeled secondary antibody at a dilution of 1:10,000. The avidin-labeled peroxidase was used at a dilution of 1:15,000. Finally three washes of 10 min each were performed with TBS-Tween, and the detection was carried out with enhanced chemiluminescence on a ChemiGenius$^2$ bioimaging system (Syngene).

### *Protein Identification by Mass Spectrometry*

After running 10% SDS-PAGE, proteins were silver-stained according to the protocol described previously (23). Protein bands of interest were trypsin-digested and analyzed as described by Slomianny *et al.* (24). Nano-LC-nano-ESI-MS/MS analyses were performed on an ion trap mass spectrometer (LCQ Deca XP$^+$, Thermo Electron, San Jose, CA) equipped with a nanoelectrospray ion source

coupled with a nano-high pressure liquid chromatography system (LC Packings Dionex, Amsterdam, The Netherlands).

1.4 $\mu$l of sample were injected into the mass spectrometer using a Famos autosampler (LC Packings Dionex). The digest was first desalted and then concentrated on a reserve phase precolumn of 0.3-mm inner diameter $\times$ 5 mm (Dionex) by solvent A (95% $H_2O$, 5% acetonitrile, 0.1% HCOOH) delivered by a Switchos pumping device (LC Packings Dionex) at a flow rate of 10 $\mu$l·min$^{-1}$ for 3 min. Peptides were separated on a 15-cm $\times$ 75-$\mu$m-inner diameter, 3-$\mu$m $C_{18}$ PepMap column (Dionex). The flow rate was set at 200 nl·min$^{-1}$. Peptides were eluted using a 5–70% linear gradient of solvent B (20% $H_2O$, 80% acetonitrile, 0.08% HCOOH) for 45 min.

Coated nanoelectrospray needles were obtained from New Objective (Woburn, MA). Spray voltage was set at 1.5 kV, and capillary temperature was set at 170 °C. The mass spectrometer was operated in positive ionization mode. Data acquisition was performed in a data-dependent mode consisting of alternately in a single run a full-scan MS over the range *m/z* 500–2000 and a full-scan MS/MS of the ion selected in an exclusion dynamic mode (the most intense ion is selected and excluded for further selection for a duration of 3 min). MS/MS data were acquired using a 2-*m/z* unit ion isolation window and a 35% relative collision energy. MS/MS .raw data files were transformed in .dta files with Bioworks 3.1 software (Thermo Electron). The .dta files generated were next merged with merge.bat software to be downloaded in Mascot software (version 2.2) to create a merge.txt file for database searches in Swiss-Prot 53.2 (updated June 26, 2007; 272,212 sequences and 99,940,143 residues) and MSDB (updated August 31, 2006; 3,239,079 sequences and 1,079,594,700 residues). Search parameters were the following: *X. laevis* for taxonomy, one missed cleavage allowed, carbamidomethylcysteine as fixed modification, 2 Da for peptide tolerance, and 0.8 Da for MS/MS tolerance. Results were scored using the probability-based Mowse (molecular weight search) score (protein score is $-10 \times \log(p)$ where $p$ is the probability that the observed match is a random event). Individual scores greater than 31 in MSDB and 23 in Swiss-Prot were considered as significant ($p < 0.05$). When peptides matched to multiple members of a protein family with the same set of peptides, the same sequences, and the same scores (for proteins and for peptides), we reported the first listed protein with its corresponding accession number that was given by the database.

### *Localization of the O-GlcNAcylation Sites on β-Actin Using MALDI-TOF/TOF*

MALDI-TOF/TOF spectra were obtained using an ULTRAFLEX III™ mass spectrometer (Bruker Daltonics GmbH, Bremen, Germany). The instrument was operated in a reflector-positive mode. Sample preparation was performed with the dried droplet method using a mixture of 0.5 $\mu$l of sample with 0.5 $\mu$l of matrix solution. The matrix solution was prepared from a saturated solution of $\alpha$-cyano-4-hydroxycinnamic acid in $H_2O$, 50% acetonitrile. External mass calibration was performed using a commercially prepared standard mixture of eight peptides (Bruker Daltonics GmbH). For each MALDI analysis, spectra were acquired using the FlexControl™ acquisition software (Version 2.2, Bruker Daltonics GmbH).

### *Immunocytological Analysis*

Immunocytological analyses were carried out as described elsewhere (7, 25).

*Hemisection of Oocytes*—All steps were done in 1.5-ml microcentrifuge tubes. The oocytes were fixed overnight in methanol at −20 °C. Samples were gradually rehydrated with PBS. After five rinses in PBS, the samples were incubated in PBS containing 0.1% (v/v) Tween 20 and 3% (w/v) BSA for 30 min followed by an overnight incubation at 4 °C with the primary antibodies in PBS, 0.1% (v/v) Tween 20, 3% (w/v) BSA (diluted 1:50 for the anti-$\beta$-tubulin (Tub2.1), anti-OGT (DM17), and anti-*O*-GlcNAc (CTD110.6 or RL2)). Samples were then rinsed five times with PBS and incubated for 1 h at 4 °C with the Alexa Fluor 488 goat anti-mouse IgG, Alexa Fluor 488 goat anti-rabbit IgG, Alexa Fluor 594 goat anti-rabbit IgG, or Texas Red-labeled anti-mouse IgM secondary antibodies (1:100 in PBS, 0.1% (v/v) Tween 20, 3% (w/v) bovine serum albumin). After five rinses in PBS, samples were cut in half at the animal-vegetal equator. The vegetal half was discarded, and the animal half was transferred to a standard slide. The samples were dried and mounted in 80% glycerol, 20% PBS containing 1 $\mu$g·ml$^{-1}$ Hoechst 33342. The oocytes were visualized using an Axioplan 2 imaging microscope (Zeiss) and an Axio Cam HRc camera (AxioVision).

*7-$\mu$m Sections of Oocytes*—The oocytes were fixed overnight in methanol at −20 °C. Methanol was then gradually replaced by butanol before embedding in paraffin. 7-$\mu$m sections were cut and transferred to a standard slide. Paraffin was removed with methylcyclohexane, and samples were gradually rehydrated in successive baths of alcohol ranging from 100 to 70% and finally water. After three rinses in PBS, indirect immunofluorescence analyses were carried out as described above.

## RESULTS

*Classical Techniques of O-GlcNAc-bearing Protein Enrichments Are Not Suitable for Large Scale Identification in Oocyte*—We have reported previously that the *X. laevis* oocyte $G_2$/M transition was accompanied by an increase in *O*-GlcNAc glycosylation (8, 9). This glycosylation status change could be observed using either the anti-*O*-GlcNAc-specific RL2 or CTD110.6 antibodies (Fig. 1, *A* and *B*, respectively) and wheat germ agglutinin (Fig. 1*C*), a lectin that recognizes non-reducing terminal GlcNAc residues. These three tools are frequently used for the purification of *O*-GlcNAc-modified proteins with the intention of their identification (26, 27). Unfortunately this classical approach was not adequate to identify *O*-GlcNAcylated proteins in *X. laevis* oocyte. Indeed *Xenopus* oocytes express much lower amounts of *O*-GlcNAc than the typical somatic cell (HeLa) when compared for equal proteins quantities (Fig. 1*D*, *top panel* (*O*-GlcNAc staining) and *bottom panel* (tubulin staining); compare the expression of $\alpha$-tubulin between immature oocytes, matured oocytes, and HeLa). Even working with high amounts of oocytes (several milligrams of total proteins), it was difficult to obtain sufficient quantities of *O*-GlcNAcylated proteins for their identification by the proteomics approach. The only way to reach this objective was to enrich *O*-GlcNAcylated proteins using anti-*O*-GlcNAc antibodies (or with WGA) and by staining the bound proteins with specific antibodies or by immunoprecipitating the protein of interest followed by its staining with an anti-*O*-GlcNAc antibody (Fig. 2, *A* and *B*). Following these directed/targeted approaches, anti-actin immunoprecipitations (Fig. 2*A*) and WGA bead enrichments (Fig. 2*B*) were performed on immature and matured *Xenopus* oocytes crude extracts, and bound proteins were analyzed by Western blot.

Using this strategy, we first identified actin, a major cytoskeleton protein (Fig. 2*A*) as an *O*-GlcNAc-bearing protein.

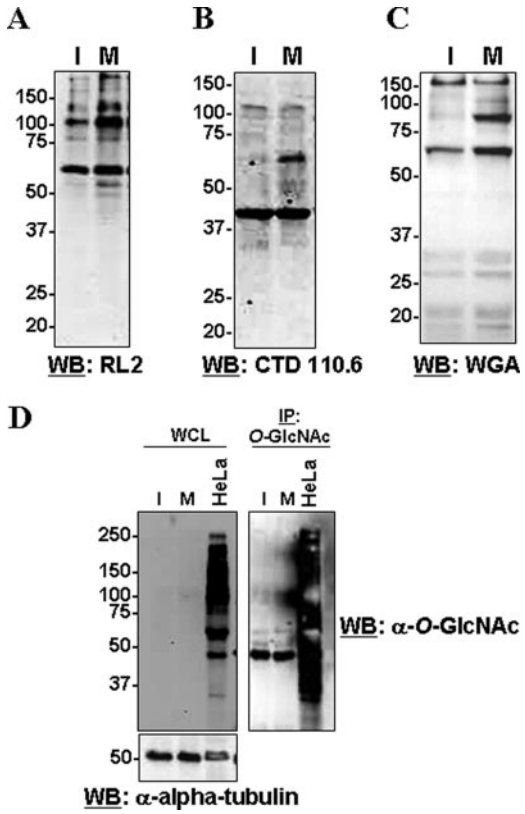


FIG. 1. **Matured *X. laevis* oocyte expresses low *O*-GlcNAc amounts limiting the identification of glycosylated proteins.** *A*, *B*, and *C*, progesterone stimulation induces an *O*-GlcNAcylation content increase in oocyte. Meiotic resumption was triggered by stimulating immature oocytes with progesterone (see the Introduction for more details). Progesterone is naturally produced and secreted by follicular cells surrounding the oocyte after their stimulation with the hypophyseal gonadotropin LH. M phase entry was scored as described under "Experimental Procedures." Immature ($G_2$-arrested) and matured (M phase-entered) oocytes were lysed in homogenization buffer. Proteins were separated by SDS-PAGE and electroblotted onto nitrocellulose, and *O*-GlcNAcylation was analyzed by Western blot using the anti-*O*-GlcNAc-directed antibodies RL2 (*A*) and CTD110.6 (*B*) or HRP-labeled WGA (*C*). *D*, *Xenopus* oocyte contains very low amounts of *O*-GlcNAc. Immature oocytes, matured oocytes, and HeLa cells were analyzed according to their *O*-GlcNAc content using the RL2 anti-*O*-GlcNAc antibody. This analysis was performed both on whole cell lysates (*left panel*) and on *O*-GlcNAc-enriched fractions (*right panel*). An anti-α-tubulin was used on the whole cell lysate to show the equal quantity of proteins loaded per lane. Protein mass markers are indicated at the *left* (kDa). *I*, immature oocytes; *M*, matured oocytes; *WB*, Western blot; *IP*, immunoprecipitation; *WCL*, whole cell lysate.

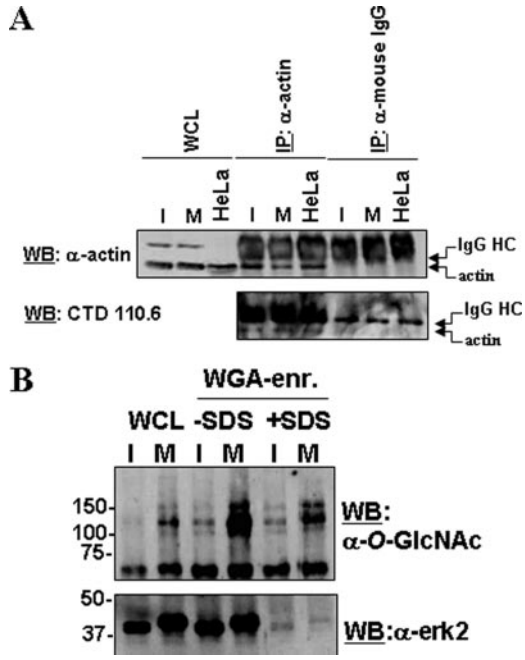


FIG. 2. **Actin and erk2 bear *O*-GlcNAc residues.** *A*, immature oocytes, matured oocytes, and HeLa cells were lysed in the immunoprecipitation buffer. Immunoprecipitation of actin was performed as described under "Experimental Procedures." After running, the immunoprecipitates were stained either with the anti-actin or the anti-*O*-GlcNAc antibodies. Controls of immunoprecipitation were carried out with normal rabbit IgG. *B*, immature and matured oocytes were lysed in the homogenization buffer, and the enrichments of the *O*-GlcNAc proteins on WGA-agarose (*WGA-enr.*) were performed either in non-denaturing conditions (−*SDS*) or in harsh conditions (+*SDS*) as described under "Experimental Procedures." Bound proteins were analyzed using the anti-*O*-GlcNAc and the anti-erk2 antibodies. Protein mass markers are indicated at the *left* (kDa). *I*, immature oocytes; *M*, matured oocytes; *WB*, Western blot; *WCL*, whole cell lysate; *IP*, immunoprecipitation; *IgG HC*, immunoglobulin heavy chain.

Using WGA enrichment in non-denaturing and harsh conditions, we demonstrated previously that Hsp/Hsc70 was *O*-GlcNAcylated and that cyclin B2 was associated with an *O*-GlcNAcylated partner (9). Following the same approach, we showed the *O*-GlcNAc modification of erk2 (Fig. 2*B*). At this stage, we concluded that the use of anti-*O*-GlcNAc antibodies or lectins was limited for the identification of *O*-GlcNAcylated proteins in *Xenopus* oocytes. For these reasons we developed another approach based on an *in vitro* enzymatic labeling (Fig. 3).

*Both Structural and Functional Proteins Have Higher O-GlcNAcylation Levels in Matured Oocyte*—β1,4-Galactosyltransferase I (GalT1) catalyzes the transfer of galactose to non-reductive terminal GlcNAc residues. In the presence of α-lactalbumin, GalT1 is capable to elongate glucose to form lactose. GalT1 can also transfer GalNAc from UDP-GalNAc to form low amounts of GalNAc β1,4-GlcNAc. The study of these differences of activities led to the engineering of Y289L GalT1 (28) allowing this mutant galactosyltransferase to enlarge its specificity for synthetic donors such as UDP-Gal analogues like UDP-2-deoxy-2-propanonyl-Gal (29). The chemical labeling of 2-deoxy-2-propanonyl-Galβ1,4-GlcNAc proteins with biotin enables their detection with avidin-labeled peroxidase. UDP-GalNAz, another UDP-Gal derivative, is also a substrate for the Y289L GalT1 that can transfer GalNAz to *O*-GlcNAc residues. This enzymatic labeling is followed by the chemical addition of a biotin alkyne probe. Indeed in the presence of

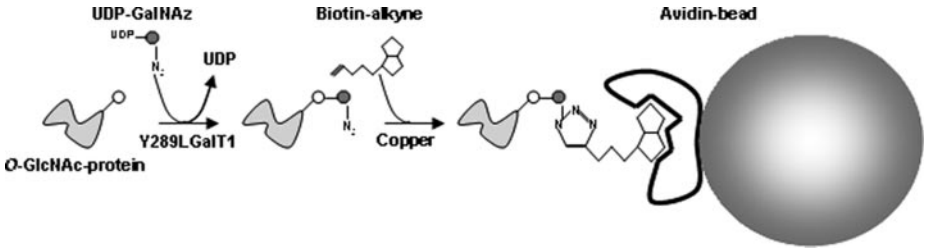


FIG. 3. **The UDP-GalNAz and biotin alkyne labeling procedure.** Labeling of the *O*-GlcNAc-bearing proteins by GalNAz and biotin alkyne was carried out using the Click-it *O*-GlcNAc enzymatic labeling system and the Click-it glycoprotein detection kit (Invitrogen) as described under "Experimental Procedures." Briefly mutant GalT1 (Y289L GalT1) transfers GalNAz from the synthetic donor UDP-GalNAz to target the *O*-GlcNAcylated proteins to form GalNAz $\beta$1,4-GlcNAc proteins. This enzymatic labeling is followed by the chemical addition of a biotin alkyne probe in the presence of Cu(I) to form a stable triazole derivative. Biotinylated GalNAz-*O*-GlcNAc proteins were then purified on avidin beads.

Cu(I), azides and alkynes react together to form stable triazole derivatives (cycloaddition) (30). In conjunction with $\beta$-elimination followed by a Michael addition with DTT, this labeling has enabled the identification of a major site of *O*-GlcNAc glycosylation (Ser-55) on the intermediate filament vimentin (31). Therefore, immature and matured oocytes were lysed in homogenization buffer, and *O*-GlcNAc residues were *in vitro* elongated by GalNAz and subsequently biotinylated with or without further enrichment on avidin beads as described in Fig. 3. Control experiments were performed in parallel on bovine $\alpha$-crystallin that contains a single *O*-GlcNAc residue on Ser-162 (Fig. 4*A*). The proteins were separated by SDS-PAGE, electrotransferred, and stained with peroxidase-labeled avidin (Fig. 4*A*). For further identification of the biotin-labeled proteins (Fig. 4*A*), avidin-enriched biotinylated proteins were separated by SDS-PAGE and silver-stained (Fig. 4*B*). The bands were cut up and trypsin-digested. The peptides were extracted, desalted, and analyzed by nano-LC-nano-ESI-MS/MS (for details see "Experimental Procedures"). These mass spectrometry analyses allowed for the identification of 23 proteins that are listed in Table I according to their biological role, *i.e.* structural proteins, metabolic enzymes, translational proteins, and other functions. Several of these proteins were already identified as bearing *O*-GlcNAc residues, but none were described previously in *Xenopus* (see the "Discussion" for details).

To check that the proteins identified by the enzymatic/chemical approach bound specifically to avidin, control experiments were performed. In this respect, proteins from matured oocytes were labeled with GalNAz, but the labeling with the biotin alkyne was omitted. Labeled proteins were enriched on avidin-coupled beads, and the profile of the bound proteins was analyzed by a staining with the avidin-labeled peroxidase and compared with the profile of the double labeled proteins (Fig. 4*C*). The same experiment was also performed without any labeling (neither the enzymatic labeling nor the chemical labeling). Apart from proteins with molecular masses higher than 60 kDa (indicated by *NS* (nonspecific)) and that could correspond to natural biotinylated proteins such as acetyl-CoA carboxylase, none of the bands found in the avidin-enriched fraction was found in the control fractions (with no labeling or only labeled with GalNAz). Similar controls were performed on $\alpha$-crystallin, which could be detected on the enriched fraction only when the double labeling was performed (Fig. 4*C*, *left part* of the *bottom panel*).

We also confirmed the *O*-GlcNAc modification of PCNA and PP2A, identified by the proteomics approach (Table I); actin, identified both by the proteomics approach and by immunoprecipitation (Table I and Fig. 2*A*); and erk2, visualized with the WGA bead enrichment (Fig. 2*B*): Fig. 4*D* reveals that these proteins can be detected on the avidin-enriched fraction by Western blot only in the double labeling conditions. To confirm the glycosylation of erk2, proteins were doubly labeled with GalNAz and biotin, and erk2 was subsequently immunoprecipitated. The *O*-GlcNAcylation of the bound erk2 was revealed by Western blot using avidin-peroxidase (Fig. 4*E*).

One MS/MS spectrum for actin and tubulin, two proteins implicated in cell shape and architecture, is presented in Fig. 5. The sequence localization of the identified peptides is indicated in the primary sequence of each protein.

*A Major O-GlcNAcylation Site Maps in the Region 318–324 of $\beta$-Actin*—As previously indicated, $\alpha$-crystallin was used as a standard to validate the methodology of the GalNAz/biotin alkyne labeling procedure in our attempts to map *O*-GlcNAcylation sites. $\alpha$-Crystallin (Swiss-Prot accession number P02470) possesses one site of *O*-GlcNAcylation on serine 162. The theoretical molecular mass of the modified peptide is 1641.84 Da after trypsin digestion and one missed cleavage: the sequence of the peptide is AIPVS$^{162}$REEKPSSAPSS. The MALDI-TOF/TOF spectrum of the $\alpha$-crystallin peptide *m/z* 2617.268 (Fig. 6) showed a neutral loss of 975.310 Da between the precursor ion *m/z* 2617.268 and the $y_{16}$ ion *m/z* 1641.958 corresponding to the modification with GlcNAc/GalNAz/biotin. This result confirmed the presence of the modified form of $\alpha$-crystallin and allowed us to validate the biotin alkyne labeling procedure in the mapping of *O*-GlcNAcylation sites. A sample in which $\beta$-actin was identified was analyzed by LC-MALDI-TOF/TOF using similar experimental conditions. Two ions corresponding to peptides derived from the same sequence of the $\beta$-actin were detected in the MS spectra (Table II). MS/MS analysis of these ions was not performed because of the low signal intensity on the MS spectrum. Despite low expression of

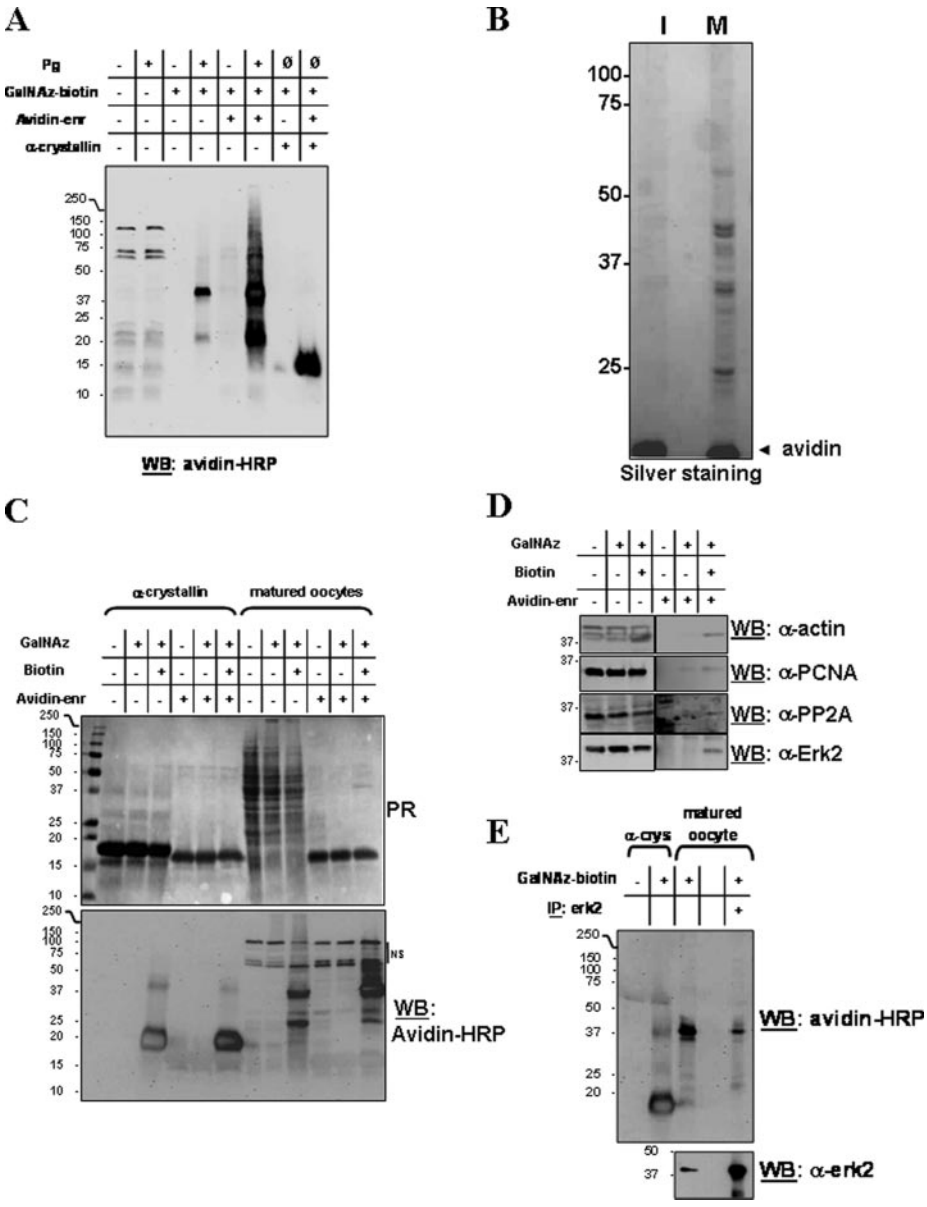


FIG. 4. **Labeling of the *Xenopus* oocyte *O*-GlcNAc-bearing proteins by GalNAz and biotin alkyne.** *A*, after labeling of the *Xenopus* oocytes (immature and matured) *O*-GlcNAcylated proteins and enrichment of the labeled proteins on avidin-coupled beads using the procedure described in Fig. 3, bound proteins were separated by SDS-PAGE, and Western blot analyses were performed using HRP-labeled avidin to test the efficiency of the labeling and of the enrichment procedures. α-Crystallin was used as a positive control. *B*, after enzymatic and chemical labeling, immature and matured oocyte *O*-GlcNAcylated proteins were enriched on avidin beads, separated by SDS-PAGE, and silver-stained. Each band was excised and subjected to trypsin digestion for further mass spectrometry analyses. *C*, controls of labeling and controls of the avidin bead enrichment were carried out on α-crystallin and on matured oocytes. The proteins were separated by SDS-PAGE, stained with Ponceau red (*PR*), and destained with TBS-Tween. The membrane was saturated with bovine serum albumin, and then a staining was performed with the avidin-labeled peroxidase. *D*, to directly bring to the fore the *O*-GlcNAcylation of three of the proteins found by the analyses of the mass spectrometry data, avidin-bound proteins were separated by SDS-PAGE and probed with anti-actin, anti-PCNA, and anti-PP2A antibodies. On the same figure, the staining of the avidin-bound proteins with the anti-erk2 antibodies is also shown. *E*, after labeling of the matured oocyte *O*-GlcNAcylated proteins, an immunoprecipitation was specifically performed with the anti-erk2 antibodies. The immunopurified erk2 was stained either with the avidin-labeled HRP or with the anti-erk2 antibodies. Protein mass markers are indicated at the *left* (kDa). *Pg*, progesterone; *I*, immature oocytes; *M*, matured oocytes; *avidin-enr*, avidin bead-enriched proteins; *WB*, Western blot; *IP*, immunoprecipitation; *crys*, crystallin; *NS*, nonspecific bands.

*O*-GlcNAcylation in the *Xenopus* oocyte, these analyses enabled the mapping of an *O*-GlcNAcylation site in a region of β-actin between amino acids 318 and 324.

*The Meiotic Spindle is O-GlcNAc-modified and/or Is Associated with O-GlcNAc Proteins and Interacts with OGT*—Because we identified β-tubulin as an *O*-GlcNAc-modified

TABLE I

*X. laevis oocyte proteins identified by mass spectrometry using the GalNAz/biotin double labeling*

The accession number, the bank used for the identification, the protein name, the apparent molecular mass found in SDS-PAGE, the theoretical molecular mass, the percentage of coverage, the Mascot score, and the number of peptides for each protein are reported. For each peptide, the charge state, the observed precursor *m/z* (Obs. *M*), the experimental (Exp. *M*) and theoretical (Cal. *M*) precursor neutral masses, the delta mass (Δ*M*), the number of missed cleavages, the peptide score value delivered by Mascot, and the peptide sequence are indicated. References in the last column of the table indicate the study relating the first description of the protein as bearing *O*-GlcNAc moieties.

| Accession number | Bank name | Protein name | Apparent molecular mass | Theoritical molecular mass | Coverage | Mascot score | Number of peptides | Charge | Obs. *M* | Exp. *M* (molecular weight) | Cal. *M* | Δ*M* | Missed cleavages | Score, peptide | Sequence | Previous *O*-GlcNAc description |
|---|---|---|---|---|---|---|---|---|---|---|---|---|---|---|---|---|
| | | | *Da* | *Da* | % | | | | | | | | | | | |
| Cell shape and architecture | | | | | | | | | | | | | | | | |
| TBB4_XENLA | Swiss-Prot | Tubulin β-4 chain | 54,950 | 50,240 | 12 | 259 | 5 | 2 | 572.7 | 1143.39 | 1142.62 | 0.7688 | 0 | 55 | K ↓ LAVNMVPFPR ↓ L | |
| | | | | | | | | 2 | 665.1 | 1328.18 | 1327.64 | 0.5449 | 0 | 53 | R ↓ INVYYNEATGGK ↓ Y | |
| | | | | | | | | 2 | 801.81 | 1601.61 | 1600.81 | 0.7984 | 0 | 68 | R ↓ AVLVDLEPGTMDSVR ↓ S | |
| | | | | | | | | 2 | 846.71 | 1691.41 | 1690.86 | 0.5564 | 0 | 76 | R ↓ ALTVPELTQQMFDAK ↓ N | |
| | | | | | | | | 2 | 923.01 | 1844 | 1842.92 | 1.0828 | 1 | 92 | R ↓ INVYYNEATGGKYVPR ↓ A | |
| ACTB_XENLA | Swiss-Prot | β-Actin | 42,240 | 42,082 | 17 | 154 | 5 | 2 | 519.19 | 1036.38 | 1035.64 | 0.7399 | 1 | 21 | K ↓ IKIIAPPER ↓ K | 32 |
| | | | | | | | | 2 | 567.19 | 1132.37 | 1131.51 | 0.8549 | 0 | 51 | R ↓ GYSFTTTAER ↓ E | |
| | | | | | | | | 2 | 759.52 | 1517.04 | 1515.69 | 1.3477 | 0 | 52 | K ↓ QEYDESGPSIVHR ↓ K | |
| | | | | | | | | 2 | 896.25 | 1790.5 | 1789.88 | 0.6171 | 0 | 60 | K ↓ SYELPDGQVITIGNER ↓ F | |
| | | | | | | | | 2 | 977.83 | 1953.64 | 1953.06 | 0.5911 | 0 | 54 | R ↓ VAPEEHPVLLTEAPLNPK ↓ A | |
| Metabolism | | | | | | | | | | | | | | | | |
| O129758XENLA | MSDB | Aldolase | 39,660 | 39,381 | 6 | 135 | 3 | 2 | 533.23 | 1064.45 | 1063.55 | 0.9033 | 0 | 56 | R ↓ QLLFTADEK ↓ V | |
| | | | | | | | | 2 | 667.32 | 1332.63 | 1331.69 | 0.9403 | 0 | 66 | K ↓ GILAADESTGSIAK ↓ R | |
| | | | | | | | | 2 | 745.54 | 1489.08 | 1487.79 | 1.2897 | 1 | 72 | K ↓ GILAADESTGSIAKR ↓ L | |
| G3P_XENLA | Swiss-Prot | Glyceraldehyde-3-phosphate dehydrogenase | 44,680 | 36,017 | 28 | 265 | 5 | 1 | 869.65 | 868.64 | 868.5 | 0.1473 | 0 | 22 | K ↓ VIPELNGK ↓ I | 26, 27 |
| | | | | | | | | 1 | 1355.75 | 1354.74 | 1354.72 | 0.0271 | 0 | 35 | R ↓ GAGQNIIPASTGAAK ↓ A | |
| | | | | | | | | 2 | 779.42 | 1556.83 | 1555.8 | 1.0343 | 0 | 88 | R ↓ VPTPNVSWDLTCR ↓ L | |
| | | | | | | | | 2 | 844.75 | 1687.49 | 1686.93 | 0.5621 | 0 | 65 | K ↓ LIINDQVITVFQER ↓ D | |
| | | | | | | | | 3 | 870.04 | 2607.12 | 2605.32 | 1.8032 | 0 | 59 | K ↓ VINDNFGIVEGLMTTVHAFTATQK ↓ T | |
| ENOA_XENLA | Swiss-Prot | α-Enolase | 51,400 | 47,930 | 2 | 48 | 1 | 2 | 572.49 | 1142.96 | 1142.6 | 0.3615 | 0 | 48 | R ↓ IGAEVYHNLK ↓ N | 26, 27 |
| KPYK_XENLA | Swiss-Prot | Pyruvate kinase | 62,330 | 57,489 | 12 | 184 | 6 | 1 | 856.68 | 855.68 | 855.51 | 0.1648 | 0 | 26 | R ↓ APIISVTR ↓ N | 26 |
| | | | | | | | | 1 | 964.72 | 963.71 | 963.55 | 0.1608 | 0 | 19 | R ↓ GIFPVLYR ↓ E | |
| | | | | | | | | 2 | 546.28 | 1090.55 | 1089.59 | 0.9632 | 1 | 16 | R ↓ QLFEELRR ↓ V | |
| | | | | | | | | 2 | 614.77 | 1227.53 | 1226.65 | 0.8831 | 0 | 74 | R ↓ LDIDSEPIVAR ↓ N | |
| | | | | | | | | 2 | 797.57 | 1593.13 | 1591.77 | 1.3624 | 0 | 70 | R ↓ DPTEATAVGAVEASFK ↓ C | |
| | | | | | | | | 2 | 807.92 | 1613.83 | 1612.71 | 1.1194 | 0 | 60 | R ↓ EAVHEAWAEDVDSR ↓ V | |
| Q5XGY5_XENLA | MSDB | Pyruvate dehydrogenase PdhE1β-2 protein | 31,570 | 39,595 | 4 | 95 | 1 | 2 | 902.01 | 1802.02 | 1800.89 | 1.1304 | 0 | 95 | R ↓ VFLLGEEVAQYDGAYK ↓ I | |
| LDHA_XENLA | Swiss-Prot | L-Lactate dehydrogenase A chain | 31,420 | 36,925 | 8 | 83 | 2 | 2 | 602.57 | 1203.12 | 1202.62 | 0.5009 | 0 | 83 | R ↓ IIGSGTNLDSAR ↓ F | |
| | | | | | | | | 2 | 857.92 | 1713.83 | 1712.91 | 0.9166 | 1 | 16 | R ↓ IVWTGGVRQQEGESR ↓ L | |
| LDHB_XENLA | Swiss-Prot | L-Lactate dehydrogenase B chain | 31,570 | 36,335 | 22 | 313 | 7 | 1 | 943.7 | 942.69 | 942.59 | 0.1073 | 0 | 28 | K ↓ FIIPQWK ↓ Y | |
| | | | | | | | | 2 | 562.46 | 1122.91 | 1121.59 | 1.3202 | 0 | 60 | K ↓ WDSAYEVIK ↓ L | |
| | | | | | | | | 2 | 567.21 | 1132.42 | 1131.59 | 0.8307 | 0 | 50 | K ↓ SAETLWGIQK ↓ D | |
| | | | | | | | | 2 | 844.36 | 1686.71 | 1684.87 | 1.8367 | 0 | 63 | K ↓ ELADELALVDILEDK ↓ L | |
| | | | | | | | | 3 | 606.29 | 1815.86 | 1813.97 | 1.8938 | 1 | 43 | K ↓ LKGEVMDLQHGSLFLK ↓ T | |
| | | | | | | | | 2 | 919.86 | 1837.71 | 1836.92 | 0.7973 | 1 | 85 | K ↓ TPTIVADKDYSVTANSR ↓ I | |
| | | | | | | | | 2 | 964.56 | 1927.11 | 1926.05 | 1.0615 | 1 | 65 | K ↓ ELADELALVDILEDKLK ↓ G | |

TABLE I—*continued*

| Accession number | Bank name | Protein name | Apparent molecular mass | Theoritical molecular mass | Coverage | Mascot score | Number of peptides | Charge | Obs. *M* | Exp. *M* (molecular weight) | Cal. *M* | Δ*M* | Missed cleavages | Score, peptide | Sequence | Previous *O*-GlcNAc description |
|---|---|---|---|---|---|---|---|---|---|---|---|---|---|---|---|---|
| Q8AVH2_XENLA | MSDB | Creatine kinase isozyme IV | 39,660 | 42,442 | 11 | 101 | 3 | 2 | 617.57 | 1233.13 | 1231.6 | 1.5249 | 0 | 26 | K ↓ DLFDPIIEDR ↓ H | 27 |
| | | | | | | | | 2 | 754.78 | 1507.54 | 1506.69 | 0.8524 | 0 | 82 | K ↓ GGDDLDPNYVLSSR ↓ V | |
| | | | | | | | | 2 | 983.44 | 1964.88 | 1963.92 | 0.9591 | 0 | 44 | R ↓ GTGGVDTAAVGGVFDV-SNADR ↓ L | |
| Q918J7_XENLA | MSDB | Transketolase | 73,540 | 68,378 | 11 | 193 | 4 | 2 | 641.26 | 1280.51 | 1280.67 | −0.1651 | 0 | 21 | K ↓ ICPLVPTADAPK ↓ I | |
| | | | | | | | | 2 | 861.75 | 1721.49 | 1720.88 | 0.6161 | 0 | 86 | R ↓ SGKPTELLDMFGISAR ↓ C | |
| | | | | | | | | 2 | 1057.9 | 2113.79 | 2113.17 | 0.6133 | 0 | 63 | R ↓ VIDPFTIKPLDAATILSSGR ↓ A | |
| | | | | | | | | 2 | 1234.16 | 2466.32 | 2465.24 | 1.0803 | 1 | 60 | R ↓ TSRPDTAVIYSPEEKF-EIGQAK ↓ V | |
| Q7SZ23_XENLA | MSDB | Glutathione *S*-transferase | 24,220 | 25,546 | 34 | 138 | 6 | 1 | 962.67 | 961.66 | 961.53 | 0.1339 | 0 | 23 | K ↓ NLQAFLTR ↓ F | |
| | | | | | | | | 2 | 501.66 | 1001.31 | 1000.44 | 0.8666 | 0 | 62 | K ↓ FSCFLGDR ↓ S | |
| | | | | | | | | 2 | 675.6 | 1349.2 | 1347.68 | 1.5159 | 0 | 41 | R ↓ ILDPTCLQNFK ↓ N | |
| | | | | | | | | 2 | 794.61 | 1587.22 | 1585.78 | 1.4361 | 0 | 54 | R ↓ LLLEYTGTQYEEK ↓ L | |
| | | | | | | | | 2 | 938.57 | 1875.13 | 1873.98 | 1.1566 | 0 | 34 | K ↓ LGLDFPNLPYLVDGDVK ↓ L | |
| | | | | | | | | 3 | 748.34 | 2242.01 | 2240.07 | 1.937 | 1 | 43 | K ↓ LYVTGDAPNYDKSQ-WLNEK ↓ E | |
| SAHHA_XENLA | Swiss-Prot | Adenosylhomo-cysteinase B | 48,350 | 48,172 | 24 | 298 | 8 | 2 | 511.01 | 1020 | 1019.54 | 0.4616 | 0 | 43 | K ↓ TGVPVYAWK ↓ G | |
| | | | | | | | | 2 | 511.87 | 1021.73 | 1020.6 | 1.1255 | 0 | 40 | R ↓ HIILLAEGR ↓ L | |
| | | | | | | | | 2 | 602.21 | 1202.41 | 1201.6 | 0.8061 | 0 | 44 | K ↓ VADISLADWGR ↓ K | |
| | | | | | | | | 2 | 631.05 | 1260.09 | 1258.57 | 1.5167 | 1 | 50 | K ↓ SKFDNLYGCR ↓ E | |
| | | | | | | | | 2 | 691.46 | 1380.9 | 1379.74 | 1.1682 | 1 | 70 | K ↓ KLDEAVAAAHLDK ↓ L | |
| | | | | | | | | 2 | 825.23 | 648.44 | 1647.81 | 0.6364 | 0 | 69 | K ↓ GISEETTTGVHNLYK ↓ M | |
| | | | | | | | | 2 | 915.78 | 1829.56 | 1828.95 | 0.61 | 0 | 63 | K ↓ SSGTLQVPAINVNDSVTK ↓ S | |
| | | | | | | | | 3 | 789.91 | 2366.7 | 2365.19 | 1.5135 | 0 | 67 | K ↓ DGKPLNMILDDGGDL-TNLVHTK ↓ Y | |
| Translation | | | | | | | | | | | | | | | | |
| EF1A2_XENLA | Swiss-Prot | Elongation factor 1-α, oocyte form 3-1 | 51,400 | 50,433 | 7 | 71 | 2 | 2 | 513.59 | 1025.17 | 1024.6 | 0.5723 | 0 | 71 | K ↓ IGGIGTVPVGR ↓ V | 31 |
| | | | | | | | | 3 | 840.09 | 2517.26 | 2516.35 | 0.9099 | 0 | 7 | R ↓ VETGVLKPGMIVTF-APSNWTTEVK ↓ S | |
| RS31_XENLA | Swiss-Prot | 40 S ribosomal protein S3-A | 31,570 | 27,156 | 39 | 221 | 7 | 2 | 516.09 | 1030.17 | 1028.62 | 1.554 | 0 | 59 | R ↓ TEIIILATR ↓ T | |
| | | | | | | | | 2 | 547.23 | 1092.44 | 1091.56 | 0.8851 | 0 | 51 | K ↓ AELNEFLTR ↓ E | |
| | | | | | | | | 2 | 572.88 | 1143.74 | 1142.57 | 1.1688 | 0 | 32 | K ↓ IMLPWDPSGK ↓ I | |
| | | | | | | | | 2 | 712.7 | 1423.38 | 1422.66 | 0.7271 | 0 | 59 | R ↓ ELAEDGYSGVEVR ↓ V | |
| | | | | | | | | 2 | 787.52 | 1573.03 | 1571.75 | 1.284 | 0 | 65 | R ↓ FGFPEGSVELYAEK ↓ V | |
| | | | | | | | | 2 | 958.66 | 1915.31 | 1913.96 | 1.3483 | 0 | 32 | K ↓ AAKPDQPQPPAMPQPVATA | |
| | | | | | | | | 3 | 824.05 | 2469.13 | 2467.18 | 1.9528 | 0 | 55 | K ↓ FVDGLMIHSGDPVNY-YVDTAVR ↓ H | |
| RS32_XENLA | Swiss-Prot | 40 S ribosomal protein S3-B | 31,570 | 27,132 | 40 | 185 | 6 | 2 | 547.23 | 1092.44 | 1091.56 | 0.8851 | 0 | 51 | K ↓ AELNEFLTR ↓ E | |
| | | | | | | | | 2 | 572.88 | 1143.74 | 1142.57 | 1.1688 | 0 | 32 | K ↓ IMLPWDPSGK ↓ I | |
| | | | | | | | | 2 | 712.7 | 1423.38 | 1422.66 | 0.7271 | 0 | 59 | R ↓ ELAEDGYSGVEVR ↓ V | |
| | | | | | | | | 2 | 787.52 | 1573.03 | 1571.75 | 1.284 | 0 | 65 | R ↓ FGFPEGSVELYAEK ↓ V | |
| | | | | | | | | 2 | 965.8 | 1929.6 | 1927.98 | 1.6193 | 0 | 30 | K ↓ GAKPDQPQPPVMPQPVATA | |
| | | | | | | | | 3 | 824.05 | 2469.13 | 2467.18 | 1.9528 | 0 | 55 | K ↓ FVDGLMIHSGDPVNYY-VDTAVR ↓ H | |

TABLE I—*continued*

| Accession number | Bank name | Protein name | Apparent molecular mass | Theoritical molecular mass | Coverage | Mascot score | Number of peptides | Charge | Obs. *M* | Exp. *M* (molecular weight) | Cal. *M* | Δ*M* | Missed cleavages | Score, peptide | Sequence | Previous *O*-GlcNAc description |
|---|---|---|---|---|---|---|---|---|---|---|---|---|---|---|---|---|
| RL4A_XENLA | Swiss-Prot | 60 S ribosomal protein L4-A | 44,680 | 45,192 | 19 | 149 | 5 | 2 | 634.3 | 1266.58 | 1265.64 | 0.9461 | 1 | 61 | R ↓ KLDDLYGTWR ↓ K | |
| | | | | | | | | 2 | 635.19 | 1268.36 | 1267.75 | 0.6165 | 0 | 43 | R ↓ NIPGITLLNVSK ↓ L | |
| | | | | | | | | 3 | 520.54 | 1558.61 | 1556.73 | 1.8783 | 0 | 29 | K ↓ LAGHQTSAESWGTGR ↓ A | |
| | | | | | | | | 3 | 621.96 | 1862.86 | 1861.03 | 1.8318 | 0 | 33 | R ↓ APIRPDIVNFVHTNLR ↓ K | |
| | | | | | | | | 2 | 969.33 | 1936.64 | 1936.01 | 0.6315 | 0 | 66 | R ↓ YAVCSALAASALPALIMSK ↓ G | |
| RL5A_XENLA | Swiss-Prot | 60 S ribosomal protein L5-A | 33,910 | 34,181 | 7 | 57 | 1 | 2 | 670.41 | 1338.81 | 1337.69 | 1.1225 | 0 | 57 | K ↓ GAVDGGLSIPHSTK ↓ R | |
| RL18A_XENLA | Swiss-Prot | 60 S ribosomal protein L18-A | 23,200 | 21,735 | 5 | 56 | 1 | 2 | 571.63 | 1141.26 | 1140.62 | 0.635 | 0 | 56 | K ↓ GQNTVLLSGPR ↓ K | |
| Other function | | | | | | | | | | | | | | | | |
| PCNA_XENLA | Swiss-Prot | Proliferating cell nuclear antigen | 31,570 | 28,878 | 7 | 81 | 2 | 1 | 933.09 | 932.08 | 931.48 | 0.6052 | 0 | 31 | R ↓ YLNFFTK ↓ A | |
| | | | | | | | | 2 | 634.18 | 1266.35 | 1265.62 | 0.7294 | 0 | 72 | K ↓ FSASGELGTGNVK ↓ L | |
| TERA_XENLA | Swiss-Prot | Transitional endoplasmic reticulum ATPase | 88,830 | 89,760 | 11 | 183 | 6 | 1 | 1021.68 | 1020.68 | 1020.51 | 0.1676 | 0 | 42 | K ↓ DVDVDFLAK ↓ M | |
| | | | | | | | | 2 | 526.81 | 1051.6 | 1050.51 | 1.091 | 0 | 65 | K ↓ MDELQLFR ↓ G | |
| | | | | | | | | 2 | 587.24 | 1172.46 | 1171.66 | 0.807 | 0 | 32 | R ↓ GILLYGPPGTGK ↓ T | |
| | | | | | | | | 2 | 771.26 | 1540.52 | 1539.79 | 0.7254 | 0 | 39 | R ↓ LGDVISIQPCPDVK ↓ Y | |
| | | | | | | | | 2 | 790.32 | 1578.63 | 1577.78 | 0.8443 | 0 | 49 | K ↓ AIANECQANFISK ↓ G | |
| | | | | | | | | 2 | 913.16 | 1824.32 | 1822.91 | 1.4128 | 0 | 57 | R ↓ ELQELVQYPVEHPDK ↓ F | |
| Q7ZWU1_XENLA | MSDB | Stress-induced phosphoprotein (Hop) | 73,540 | 62,506 | 2 | 73 | 1 | 2 | 709.19 | 1416.37 | 1415.76 | 0.6111 | 0 | 73 | R ↓ VAYINPDLALEAK ↓ N | |
| JC4316 | MSDB | Phosphoprotein phosphatase 2A-$\beta$ catalytic chain | 31,420 | 36,126 | 3 | 40 | 1 | 2 | 671.34 | 1340.67 | 1339.65 | 1.0152 | 0 | 40 | K ↓ YSFLQFDPAPR ↓ R | |
| RAN_XENLA | MSDB | GTP-binding nuclear protein ran | 26,100–24,220 | 24,554 | 4 | 55 | 2 | 2 | 608.07 | 1214.14 | 1213.59 | 0.5442 | 0 | 35 | K ↓ NLQYYDISAK ↓ S | 26 |
| | | | | | | | | 2 | 648.4 | 1294.79 | 1293.59 | 1.1968 | 0 | 55 | K ↓ FNVWDTAGQEK ↓ F | |

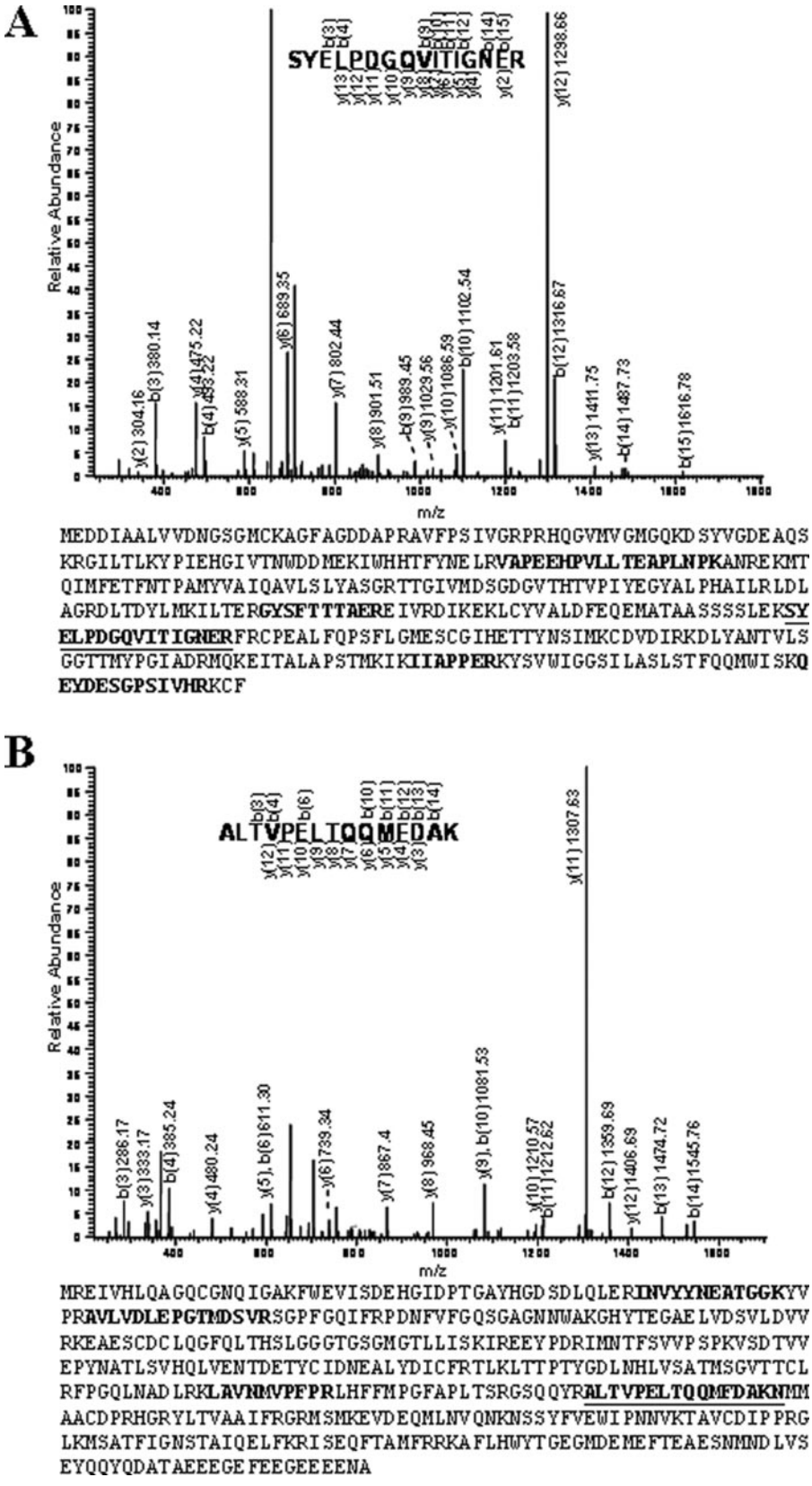


FIG. 5. **β-Actin and β-tubulin representative mass spectrometry spectra.** *A*, *top panel*, nano-LC-nano-ESI-MS/MS spectrum of the doubly charged ion *m/z* 896.25 showing one of the five sequences stemming from actin digestion; *bottom panel*, localization of the five sequences found for actin by nano-LC-nano-ESI-MS/MS are located in the actin primary structure (*bold characters*). The sequence described in the *top panel* spectrum is *underlined*. *B*, *top panel*, nano-LC-nano-ESI-MS/MS spectrum of the doubly charged ion *m/z* 846.71 showing one of the four sequences stemming from tubulin digestion; *bottom panel*, localization of the four sequences found for tubulin by nano-LC-nano-ESI-MS/MS are located in the tubulin primary structure (*bold characters*). The sequence described in the *top panel* spectrum is *underlined*.

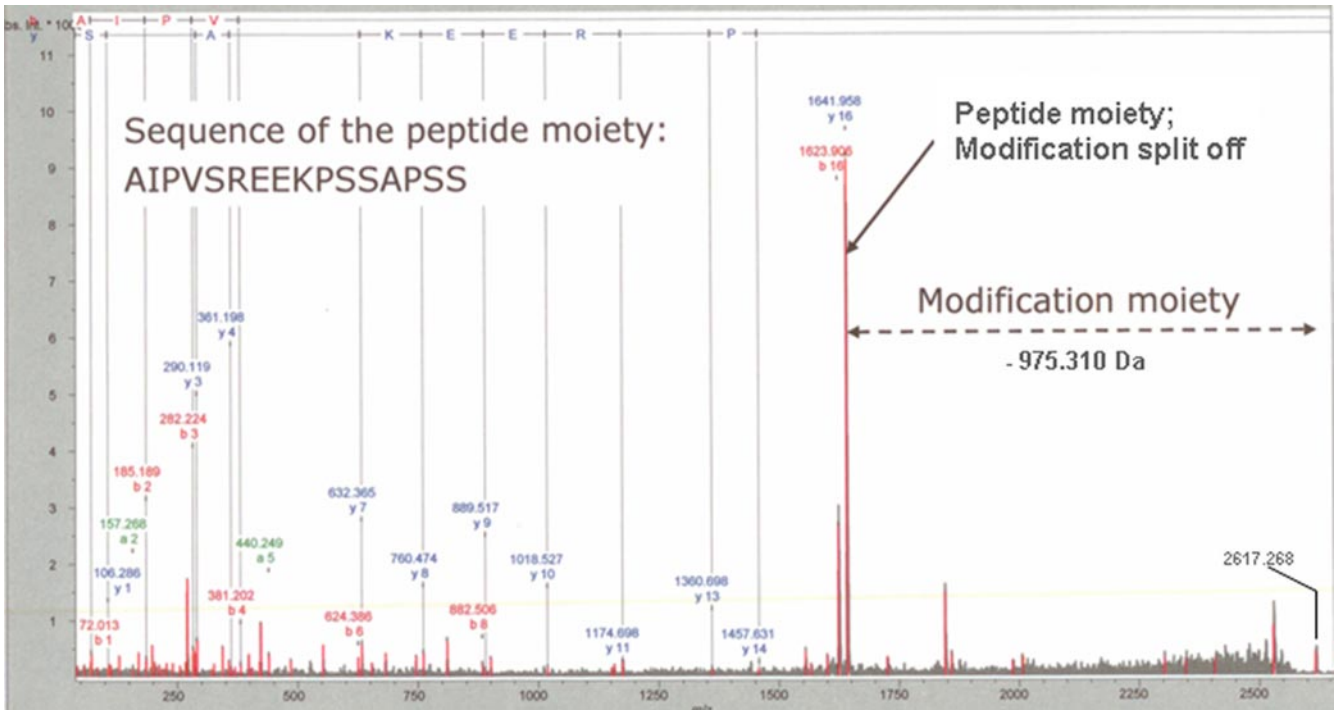


FIG. 6. **MALDI-TOF/TOF spectrum of $\alpha$-crystallin modified peptide (*m/z* 2617.268 selected).** A neutral loss of 975.310 Da is observed between the precursor ion and the $y_{16}$ ion. This loss corresponds to the modification of the peptide with GlcNAc/GalNAz/biotin. The peptide sequence of $\alpha$-crystallin was confirmed by MS/MS (*left* of the figure).

TABLE II

*Characteristics of the two $\beta$ -actin modified peptides*

The sequences corresponding to each tryptic peptide are indicated with the positions of the first and the last amino acids. $M_{ox}$ indicates methionine oxidation, and * indicates the potential site of *O*-GlcNAcylation. For each peptide, the number of missed cleavages, the theoretical precursor ion *m/z* peptide, and the theoretical precursor ion of the peptide with biotin/GalNAz/*O*-GlcNAc labeling are presented.

| Peptide | Missed cleavages | Theoretical precursor ion *m/z* | Theoretical precursor ion *m/z* with biotin/GalNAz/*O*-GlcNAc labeling |
|---|---|---|---|
| $^{316}$EITALAPST*$M_{ox}$K$^{326}$ | 0 | 1177.6133 | 2153.1733 |
| $^{313}$MQKEITALAPST*MK$^{326}$ | 1 | 1548.8124 | 2524.3724 |

protein by proteomics approach and because tubulins are major components of the division spindle, we wanted to directly visualize the *O*-GlcNAcylation of the spindle.

For that purpose, the metaphase II meiotic spindles from hemisections and from 7-$\mu$m sections (Fig. 7, *A* and *B*, respectively) of the matured oocytes were observed using immunofluorescence microscopy. Pictures indeed showed a colocalization of tubulins and *O*-GlcNAc indicating that the meiotic spindle is highly glycosylated and/or that it is associated with *O*-GlcNAc-bearing proteins (Fig. 7*A*, *top panel*). The same observation was made with OGT (Fig. 7*A*, *bottom panel*, and *B*, *top panel*). Slawson *et al.* (17) showed previously that OGT was found on the mitotic spindle in somatic cells, but the present work is the first to report direct *O*-GlcNAcylation of the meiotic spindle. Another interesting point is that chromosomes were highly stained with both anti-*O*-GlcNAc and anti-OGT antibodies (Fig. 7*B*, *middle* and *bottom panels*), demonstrating that DNA, at least in its condensed form, is associated with *O*-GlcNAcylated proteins. This observation is reinforced by data presented in supplemental Fig. 1 showing mitotic COS7 cells: as the mitosis progressed, the chromosomes showed growing intensity of *O*-GlcNAc staining; this is particularly evident for the prophase/metaphase transition. Moreover the presence of *O*-GlcNAcylation and of the enzyme that catalyzes the sugar transfer on the meiotic spindle and on the chromosomes should have consequences on microtubule nucleation, elongation, spindle morphogenesis, and chromosomal condensation and/or segregation to allow the cell to divide.

## DISCUSSION

The current data present the first analysis of the *Xenopus* oocyte *O*-GlcNAcome. Previous studies have shown that the maturation process, triggered by incubation with progesterone or by the injection of cytoplasm containing MPF, is accompanied by a global *O*-GlcNAcylation increase (8, 9). The

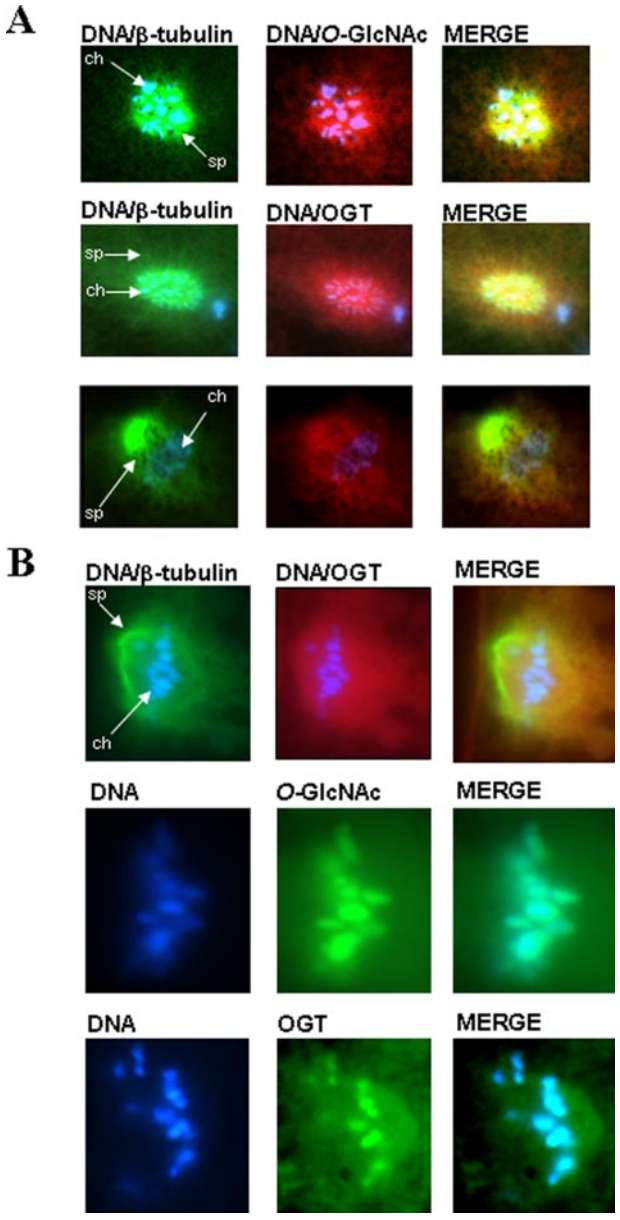


FIG. 7. **O-GlcNAc and OGT localized on the meiotic spindle and chromosomes in matured *X. laevis* oocyte.** *A*, metaphase II oocyte hemisections. Hemisections were performed as described under "Experimental Procedures." The microtubules (*sp*) were stained using anti-β-tubulin (Tub2.1), *O*-GlcNAc residues were stained using CTD110.6, OGT was stained using DM17, and the chromosomes (*ch*) were visualized using Hoechst staining. Merge pictures are shown at the *right* of the figure. *B*, metaphase II oocyte sections (7 μm). Matured oocytes were fixed, dehydrated, and embedded in paraffin. The sections (7 μm) were immunostained as described above. Merge pictures are shown at the *right* of the figure. Tubulin, OGT, and chromosomes were stained as described in *A* with the exception that OGT appears *green* at the *bottom* of the figure because we used Alexa Fluor 488 goat anti-rabbit IgG as the secondary antibody. *O*-GlcNAc residues were stained with RL2. *sp*, spindle; *ch*, chromosomes.

*O*-GlcNAcylation burst is essential for meiotic resumption because the inhibition of OGT prevents the M phase entry in $G_2$-arrested oocytes (9). Apart from β-catenin (8, 20) and Hsp/Hsc70 (33–35) for which glycosylation has been demonstrated previously in *X. laevis*, the nature of the proteins for which *O*-GlcNAcylation increased during the $G_2$/M transition was virtually unknown, and therefore the goal of this work was to identify them. This goal hit a sizable problem: whereas the *Xenopus* oocyte contains large amounts of proteins, it only expresses very low levels of *O*-GlcNAc in comparison with somatic cells (Fig. 1*D*) (for an equivalent quantity of proteins, the difference of *O*-GlcNAcylation content between the two cell types is estimated to be between 50- and 100-fold less for the oocyte than for the HeLa cells). A strategy consisting of actin immunoprecipitations followed by a staining of the immunoprecipitates with anti-*O*-GlcNAc antibodies allowed us to demonstrate that actin is *O*-GlcNAcylated (Fig. 2*A*). The enrichment of the *O*-GlcNAcylated proteins using WGA-immobilized beads also led to the identification of erk2 (Fig. 2*B*). Unfortunately anti-*O*-GlcNAc and WGA enrichments were inefficient for the identification of *O*-GlcNAcylated proteins in *Xenopus* oocyte by classical proteomics approaches. Here we tested the labeling of *O*-GlcNAc residues using UDP-GalNAz and a recombinant galactosyltransferase (Y289L GalT1). This technique, which was used recently (31), allowed for the identification of 23 proteins that are components of the cell or that are implicated in the cellular metabolism. These proteins listed in Table I are distributed in four distinct classes; several of them were described previously to be *O*-GlcNAcylated, but none were described before in *Xenopus*.

Actin and tubulins are structural proteins involved in cell architecture and the transport of many organelles and macromolecules, but they also play a crucial role in the control of the cell cycle. Both proteins were described previously as being *O*-GlcNAc-bearing proteins (31, 32, 34). In our study, the *O*-GlcNAcylation of actin was demonstrated by (i) the staining with CTD110.6, (ii) the labeling with GalNAz/biotin (followed by a staining with actin), and (iii) the proteomics procedure (nano-LC-nano-ESI-MS/MS). The actin filaments control many events during oocyte maturation, for example the cortical spindle anchorage (for a review, see Ref. 36). Tubulin (β form) was also retrieved in our list of *O*-GlcNAcylated proteins. Unfortunately because of the weak specificity and sensitivity of some antibodies raised against *X. laevis* proteins (especially in immunoprecipitation), we failed to convincingly show the direct modification of β-tubulin by probing immunoprecipitated β-tubulin with the anti-*O*-GlcNAc antibodies. Nevertheless the tubulin *O*-GlcNAc status was strengthened by the localization of *O*-GlcNAc and OGT on the meiotic spindle (Fig. 7, *A* and *B*, *top panel*). Such an observation of an interaction of OGT with the spindle was reported previously (17). These authors also described the interaction of OGT with the midbody, a cytoplasmic remnant bridging the two daughter cells at the end of cytokinesis. We observed a

similar phenomenon in mitotic HeLa cells (supplemental Fig. 2). However, the impact of *O*-GlcNAcylation on tubulin polymerization and spindle formation remains to be determined. Our results also showed that *O*-GlcNAc-bearing proteins and OGT itself were highly associated with condensed chromatin (Fig. 7*B*, *middle* and *bottom panels*, and supplemental Fig. 1). The description of an abundant distribution of *O*-GlcNAcylation on the chromatin-associated proteins was made for the first time almost 2 decades ago (37). Authors used FITC-labeled WGA and tritiated UDP-Gal radiolabeling to demonstrate the existence of *O*-GlcNAcylation on DNA-associated proteins. It is well known that a plethora of transcription factors like Sp1 and other transcriptional machinery components are intensively modified with *O*-GlcNAcylation (38). Enzymes involving in chromatin remodeling are also *O*-GlcNAcylated as it is the case for histone deacetylase 1 (39): interestingly OGT physically interacts with histone deacetylase (38). In contrast, although a yin/yang relationship between phosphorylation and *O*-GlcNAcylation on histone H3 has been proposed recently based on computer analyses (40), the direct evidence for *O*-glycosylation of histones has never been described. Personal attempts to show that such proteins were *O*-GlcNAcylated either by the use of histone-enriched fractions (supplemental Fig. 3) or by histone immunoprecipitation followed by an immunoblotting with an anti-*O*-GlcNAc antibody were unfruitful (data not shown). The supplemental Fig. 3 shows that the histones in HeLa cells do not bear any *O*-GlcNAc residues, whereas the nuclear fraction is extensively enriched in this PTM. The exact identification of the DNA-associated proteins that are modified by *O*-GlcNAcylation is one of our main challenges in the future years.

In addition to cytoskeletal proteins, we identified numerous *O*-GlcNAcylated functional proteins that can be classified in three different groups: metabolism, translation, and other functions. Among the nine enzymes involved in the cell metabolism, four play a direct role in glycolysis, namely aldolase, GAPDH, enolase, and pyruvate kinase, and two others, the $\beta$-chain 1 of the pyruvate dehydrogenase and the lactate dehydrogenase (chains A and B), both use pyruvate, the glycolysis end product, either to direct it to the citric acid cycle or to use it in anaerobic conditions (lactate dehydrogenase catalyzes the conversion of pyruvate to lactate). The pyruvate dehydrogenase $\beta$-chain 1 is the first component of the pyruvate dehydrogenase complex. It binds to the thiamine pyrophosphate to catalyze (i) the pyruvate decarboxylation and (ii) the reductive acetylation of lipoic acid. Although Guixe *et al.* (41) demonstrated the formation of ATP after injection of glucose 6-phosphate, fructose 6-phosphate, and fructose 1,6-bisphosphate and of lactate after injection of glucose, it is usually considered that glycolysis is not operational in full grown oocytes and that carbon metabolic flux is largely directed to glycogen synthesis (glycolysis only begins near gastrulation) (42, 43). The description of *O*-GlcNAcylation on glycolysis-participating enzymes is not new because it has been reported for different enzymes. Using an anti-*O*-GlcNAc antibody-containing column, Wells *et al.* (26) found that pyruvate kinase, phosphoglycerate kinase, enolase, and GAPDH were *O*-GlcNAcylated; Cieniewski-Bernard *et al.* (27) also found enolase and GAPDH to which they added the triose-phosphate isomerase. Nevertheless we describe for the first time the *O*-GlcNAcylation of aldolase. The function of *O*-GlcNAcylation on these enzymes remains to be deciphered and understood. We hypothesize that *O*-GlcNAc could take part in the regulation of glycolysis. *O*-GlcNAc itself comes from glucose utilization through the hexosamine biosynthetic pathway (for a review, see Ref. 13). If *O*-GlcNAcylation exerts a negative control on the glycolysis-regulating enzymes we can suppose that when the glycolysis is inoperative the glucose flux, in addition to being directed to glycogen synthesis at the glucose 6-phosphate crossroad, could follow the hexosamine biosynthetic pathway (fructose 6-phosphate crossroad) to produce the OGT substrate UDP-GlcNAc. Three other metabolic enzymes, namely glutathione *S*-transferase, transketolase, and *S*-adenosylhomocysteinase, have been also identified as *O*-GlcNAcylated enzymes. *S*-Adenosylhomocysteinase is an enzyme that cleaves the *S*-adenosylhomocysteine into homocysteine, a reaction product and an inhibitor of all *S*-adenosylmethionine-dependent methylation reactions. This nuclear enzyme is confined in the cytoplasm during oocyte maturation and during the early stages of the development of embryo. Then it gradually reaccumulates in the nuclei during gastrulation (44) where it participates in mRNA transcription. Because *O*-GlcNAcylation is thought to have a role in the nuclear transport of numerous proteins (for a review, see Ref. 45) and that *O*-GlcNAcylation increases during the oocyte maturation process, we can suppose that this PTM mediates the *S*-adenosylhomocysteinase subcellular localization. To test this hypothesis, it would be interesting to look at the glycosylation status of *S*-adenosylhomocysteinase during gastrulation *i.e.* when the protein is localized in the nucleus.

Numerous *O*-GlcNAcylated proteins we found are involved in translational processes. Five are ribosomal proteins, and one is the translation elongation factor eEF1. Three other ribosomal proteins were described to bear *O*-GlcNAc residues: the 40 S ribosomal S24 protein (26, 31) and the ribosomal proteins S3 and P0 (31). Little is known about the impact of *O*-GlcNAcylation on translation in comparison with the transcriptional process for which the importance of this glycosylation has been reported intensively (for reviews, see Refs. 10–14 and 38). The only significant contribution of *O*-GlcNAcylation reported for translation is the modification of p67 and its association with the $\alpha$-chain of eIF2 in the prevention of its phosphorylation by the eIF2 kinase (46). The *O*-GlcNAcylation of ribosomal proteins may be involved in the multimerization of these proteins and in their association with rRNAs to compose the ribosomal machinery. In regard to this idea, several groups have reported an implication of *O*-Glc-

NAcylation in the establishment and in the reinforcement of protein-to-protein interactions (47–49). The glycosylation of ribosomal proteins could contribute, through the formation and the stabilization of the ribosomes, to the activation of the translational machinery. In the oocyte, the transcriptional machinery is ineffective. During oogenesis, the oocyte accumulates a stock of maternal mRNAs. This stock is used to translate proteins necessary for maturation (for example, mRNA encoding mos; cyclins A1, B1, and B2; and cdk2) and also for early embryogenesis. Indeed the embryo starts to synthesize its own RNAs only at the midblastula transition. During meiotic resumption, the poly(A) tails of mRNAs are lengthened by about 100 adenyl groups. It has been demonstrated that the mRNA polyadenylation is an essential process that controls the mRNA translation (for reviews, see Refs. 50 and 51). In summary, if little is known about the regulation of translation by *O*-GlcNAcylation, we can hypothesize that *O*-GlcNAcylation may intervene at different levels (i) in the association of the different subunits constituting the ribosomal machinery, (ii) by activating/inactivating the crucial factors needed for translation, *i.e.* eIF, and (iii) indirectly by promoting the mRNA polyadenylation.

We also showed that the phosphoprotein phosphatase 2A-$\beta$ is *O*-GlcNAcylated. PP2A has been shown to negatively regulate cdc2 in $G_2$-arrested *Xenopus* oocyte, and PP2A depletion is sufficient to activate cdc2 in cell-free extract demonstrating the importance of this protein in cell cycle regulation (52). This is the second time that a phosphatase has been described as bearing *O*-GlcNAc moieties; the first one was the nuclear tyrosine phosphatase p65 (53). Recently it has been shown that PP1 $\alpha$ and $\gamma$ are in complex with OGT (54). It is therefore possible that PP2A is itself associated with OGT and that PP1 is also modified with *O*-GlcNAc residues. This hypothesis, if true, adds another dimension to the complex relationship that exists between phosphorylation and *O*-GlcNAcylation: OGT and protein phosphatases could be modified and regulated by these two PTMs, and the interaction between the two entities could tightly control the dephosphorylation and *O*-GlcNAcylation processes of targeted substrates.

A recent study reported the physical interaction of the C terminus of OGT with the MAPK p38 (55). Although the authors showed that p38 does not phosphorylate OGT and that in return OGT seems not to glycosylate the kinase, the association between the two enzymes enhances the recruitment of the OGT targets such as neurofilament H. Here we provide direct evidence of the *O*-GlcNAcylation of the MAPK p42 erk2. As mentioned previously in the Introduction, after hormonal stimulation with progesterone, two main pathways are activated, namely the p42 MAPK (mos-erk2) pathway (56) and the MPF pathway (5, 6). At this stage it is not known how the *O*-GlcNAcylation of erk2 can regulate its activity in the oocyte maturation process.

Another interesting *O*-GlcNAcylated protein identified in the study was the transitional endoplasmic reticulum ATPase (TER ATPase also known as ATPase associated with various cellular activities ATPase p97). This protein is essential for the Golgi and endoplasmic reticulum fragmentation occurring during mitosis and for the reassembly of these organelles after mitosis (for a review, see Ref. 57). A recent study describes that the cell membrane vesicular traffic is crucial for meiotic arrest (58). Golgi fragmentation blockade prevents cell division and stops the cell cycle at the $G_2$ stage. The TER ATPase is also involved in the formation of the nuclear envelope (59). The function of *O*-GlcNAc on TER ATPase activity and its impact on the Golgi, endoplasmic reticulum, and nuclear envelope fragmentation remain to be studied. We have also found that the small GTPase ran, which is implicated in the spindle assembly (60) and in the nuclear envelope reformation after division (61), was *O*-GlcNAcylated.

In conclusion, we identified several proteins belonging to four different functional groups. Although the function of *O*-GlcNAcylation has to be determined for each identified protein, our study shows that the *O*-GlcNAcylation impact in the cell cycle progression is not restricted only to key regulatory proteins like specific kinases such as erk2 or phosphatases such as PP2A. Indeed the increase in *O*-GlcNAc was found on structural proteins that could intervene in organelle displacement and fragmentation (TER ATPase and ran), in the establishment of the division spindle and its anchorage (tubulin, actin, and ran), or in the translation of mRNAs important for the maturation process (ribosomal proteins). So to highlight the role of *O*-GlcNAcylation in the cell cycle progression, it seems crucial to decipher the exact function of this PTM on each factor and especially on glycolysis enzymes.

*Acknowledgments*—We thank the "Université des Sciences et Technologies de Lille." We are grateful to Prof. Gerald W. Hart for providing us CTD110.6. We also thank Arlette Lescuyer for technical assistance. We thank the Bruker Daltonics Society for the MALDI-TOF/TOF analyses, and we are more particularly grateful to Pierre-Olivier Schmit and to Dr. Christian Rolando (headquarters of the UMR-CNRS 8009). We also thank Dr. Catherine Postic from the Cochin Institute for the final reading of the manuscript and for the grammatical corrections.

* This work was supported in part by grants from the CNRS, the "Ligue Contre le Cancer," and the "Association pour la Recherche sur le Cancer." The costs of publication of this article were defrayed in part by the payment of page charges. This article must therefore be hereby marked "*advertisement*" in accordance with 18 U.S.C. Section 1734 solely to indicate this fact.

S The on-line version of this article (available at http://www.mcponline.org) contains supplemental material.

¶ Recipient of a fellowship from the "Ministère de l'Enseignement Supérieur et de la Recherche."

‖ Both authors made equal contributions to this work and should be considered as second author.

§§ To whom correspondence should be addressed. Tel.: 3-33-20-43-44-30; Fax: 3-33-20-43-65-55; E-mail: tony.lefebvre@univ-lille1.fr.

REFERENCES

1. Malumbres, M., and Barbacid, M. (2007) Cell cycle kinases in cancer. *Curr. Opin. Genet. Dev.* **17,** 60–65

2. Masui, Y., and Markert, C. L. (1971) Cytoplasmic control of nuclear behavior during meiotic maturation of frog oocytes. *J. Exp. Zool.* **177,** 129–145
3. Masui, Y. (2001) From oocytes maturation to the in vitro cell cycle: the history of discoveries of maturation-promoting factor (MPF) and cytostatic factor (CSF). *Differentiation* **69,** 1–17
4. Ferrel, J. E., Jr. (1999) Xenopus oocyte maturation: new lessons from a good egg. *BioEssays* **21,** 833–842
5. Norbury, C., Blow, J., and Nurse, P. (1991) Regulatory phosphorylation of the p34cdc2 protein kinase in vertebrates. *EMBO J.* **10,** 3321–3329
6. Jessus, C., and Ozon, R. (2004) How does *Xenopus* oocyte acquire its competence to undergo meiotic maturation ? *Biol. Cell* **96,** 187–192
7. Bodart, J. F., Baert, F. Y., Sellier, C., Duesbery, N. S., Flament, S., and Vilain, J. P. (2005) Differential roles of p39Mos-Xp42Mpk1 cascade proteins on Raf1 phosphorylation and spindle morphogenesis in *Xenopus* oocytes. *Dev. Biol.* **283,** 373–383
8. Lefebvre, T., Baert, F., Bodart, J. F., Flament, S., Michalski, J. C., and Vilain, J. P. (2004) Modulation of *O*-GlcNAc glycosylation during *Xenopus* oocyte maturation. *J. Cell. Biochem.* **93,** 999–1010
9. Dehennaut, V., Lefebvre, T., Sellier, C., Leroy, Y., Gross, B., Walker, S., Cacan, R., Michalski, J. C., Vilain, J. P., and Bodart, J. F. (2007) *O*-Linked N-acetylglucosaminyltransferase inhibition prevents $G_2$/M transition in *Xenopus* laevis oocytes. *J. Biol. Chem.* **282,** 12527–12536
10. Hart, G. W., Housley, M. P., and Slawson C. (2007) Cycling of *O*-linked $\beta$-N-acetylglucosamine on nucleocytoplasmic proteins. *Nature* **446,** 1017–1022
11. Zachara, N. E., and Hart, G. W. (2006) Cell signaling, the essential role of *O*-GlcNAc! *Biochim. Biophys. Acta* **1761,** 599–617
12. Kudlow, J. E. (2006) Post-translational modification by *O*-GlcNAc: another way to change protein function. *J. Cell. Biochem.* **98,** 1062–1075
13. Love, D. C., and Hanover, J. A. (2005) The hexosamine signaling pathway: deciphering the "*O*-GlcNAc code". *Sci. STKE* **2005,** re13
14. Slawson, C., Housley, M. P., and Hart, G. W. (2006) *O*-GlcNAc cycling: how a single sugar post-translational modification is changing the way we think about signaling networks. *J. Cell. Biochem.* **97,** 71–83
15. Fang, B., and Miller, M. W. (2001) Use of galactosyltransferase to assess the biological function of *O*-linked N-acetyl-D-glucosamine: a potential role for *O*-GlcNAc during cell division. *Exp. Cell Res.* **263,** 243–253
16. Slawson, C., Shafii, S., Amburgey, J., and Potter, R. (2002) Characterization of the *O*-GlcNAc protein modification in *Xenopus laevis* oocyte during oogenesis and progesterone-stimulated maturation. *Biochim. Biophys. Acta* **1573,** 121–129
17. Slawson, C. Zachara, N. E., Vosseller, K., Cheung, W. D., Lane, M. D., and Hart, G. W. (2005) Perturbations in O-linked $\beta$-N-acetylglucosamine protein modification cause severe defects in mitotic progression and cytokinesis. *J. Biol. Chem.* **280,** 32944–32956
18. Berger, S. L. (2007) The complex language of chromatin regulation during transcription. *Nature* **447,** 407–412
19. Bosch, M., Cayla, X., van Hoof, C., Hemmings, B. A., Ozon, R., Merlevede, W., and Goris, J. (1995) The PR55 and PR65 subunits of protein phosphatase 2A from *Xenopus* laevis. Molecular cloning and developmental regulation of expression. *Eur. J. Biochem.* **230,** 1037–1045
20. Zhu, W., Leber, B., and Andrews, D. W. (2001) Cytoplasmic *O*-glycosylation prevents cell surface transport of E-cadherin during apoptosis. *EMBO J.* **20,** 5999–6007
21. Baert, F., Bodart, J. F., Bocquet-Muchembled, B., Lescuyer-Rousseau, A., and Vilain, J. P. (2003) Xp42(Mpk1) activation is not required for germinal vesicle breakdown but for Raf complete phosphorylation in insulin-stimulated *Xenopus* oocytes. *J. Biol. Chem.* **278,** 49714–49720
22. Chesnel, F., Bonnec, G., Tardivel, A., and Boujard, D. (1997) Comparative effects of insulin on the activation of the Raf/Mos-dependent MAP kinase cascade in vitellogenic versus postvitellogenic *Xenopus* oocytes. *Dev. Biol.* **188,** 122–133
23. Chevallet, M., Luche, S., and Rabilloud, T. (2006) Silver staining of proteins in polyacrylamide gels. *Nat. Protoc.* **1,** 1852–1858
24. Slomianny, M. C., Dupont, A., Bouanou, F., Beseme, O., Guihot, A. L., Amouyel, P., Michalski, J. C., and Pinet, F. (2006) Profiling of membrane proteins from human macrophages: comparison of two approaches. *Proteomics* **6,** 2365–2375
25. Bodart, J. F., Gutierrez, D. V., Nebreda, A. R., Buckner, B. D., Resau, J. R., and Duesbery, N. S. (2002) Characterization of MPF and MAPK activities during meiotic maturation of *Xenopus* tropicalis oocytes. *Dev. Biol.* **245,** 348–361
26. Wells, L., Vosseller, K., Cole, R. N., Cronshaw, J. M., Matunis, M. J., and Hart, G. W. (2002) Mapping sites of *O*-GlcNAc modification using affinity tags for serine and threonine post-translational modifications. *Mol. Cell. Proteomics* **1,** 791–804
27. Cieniewski-Bernard, C., Bastide, B., Lefebvre, T., Lemoine, J., Mounier, Y., and Michalski, J. C. (2003) Identification of *O*-linked N-acetylglucosamine proteins in rat skeletal muscle using two-dimensional gel electrophoresis and mass spectrometry. *Mol. Cell. Proteomics* **3,** 577–585
28. Ramakrishnan, B., and Qasba, P. K. (2002) Structure-based design of $\beta$1,4-galactosyltransferase I ($\beta$4Gal-T1) with equally efficient N-acetylgalactosaminyltransferase activity: point mutation broadens $\beta$4Gal-T1 donor specificity. *J. Biol. Chem.* **277,** 20833–20839
29. Khidekel, N., Arndt, S., Lamarre-Vincent, N., Lippert, A., Poulin-Kerstien, K. G., Ramakrishnan, B., Qasba, P. K., and Hsieh-Wilson, L. C. (2003) A chemoenzymatic approach toward the rapid and sensitive detection of *O*-GlcNAc posttranslational modifications. *J. Am. Chem. Soc.* **125,** 16162–16163
30. Wang, Q., Chan, T. R., Hilgraf, R., Fokin, V. V., Sharpless, K. B., and Finn, M. G. (2003) Bioconjugation by copper(I)-catalyzed azide-alkyne [3 + 2] cycloaddition. *J. Am. Chem. Soc.* **125,** 3192–3193
31. Wang, Z., Pandey, A., and Hart, G. W. (2007) Dynamic interplay between *O*-linked N-acetylglucosaminylation and glycogen synthase kinase-3-dependent phosphorylation. *Mol. Cell. Proteomics* **6,** 1365–1379
32. Hedou, J., Cieniewski-Bernard, C., Leroy, Y., Michalski, J. C., Mounier, Y., and Bastide, B. (2007) *O*-Linked N-acetylglucosaminylation is involved in the $Ca^{2+}$ activation properties of rat skeletal muscle. *J. Biol. Chem.* **282,** 10360–10369
33. Lefebvre, T., Cieniewski, C., Lemoine, J., Guerardel, Y., Leroy, Y., Zanetta, J. P., and Michalski, J. C. (2001) Identification of N-acetyl-D-glucosamine-specific lectins from rat liver cytosolic and nuclear compartments as heat-shock proteins. *Biochem. J.* **360,** 179–188
34. Walgren, J. L., Vincent, T. S., Schey, K. L., and Buse, M. G. (2003) High glucose and insulin promote *O*-GlcNAc modification of proteins, including $\alpha$-tubulin. *Am. J. Physiol.* **284,** E424–E434
35. Guinez, C., Lemoine, J., Michalski, J. C., and Lefebvre, T. (2004) 70-kDa-heat shock protein presents an adjustable lectinic activity towards *O*-linked N-acetylglucosamine. *Biochem. Biophys. Res. Commun.* **319,** 21–26
36. Sun, Q. Y., and Schatten, H. (2006) Regulation of dynamic events by microfilaments during oocyte maturation and fertilization. *Reproduction* **131,** 193–205
37. Kelly, W. G., and Hart, G. W. (1989) Glycosylation of chromosomal proteins: localization of O-linked N-acetylglucosamine in Drosophila chromatin. *Cell* **57,** 243–251
38. Comer, F. I., and Hart, G. W. (1999) *O*-GlcNAc and the control of gene expression. *Biochim. Biophys. Acta* **1473,** 161–171
39. Yang, X., Zhang, F., and Kudlow, J. E. (2002) Recruitment of *O*-GlcNAc transferase to promoters by corepressor mSin3A: coupling protein *O*-GlcNAcylation to transcriptional repression. *Cell* **110,** 69–80
40. Kaleem, A., Hoessli, D. C., Ahmad, I., Walker-Nasir, E., Nasim, A., Shakoori, A. R., and Din, N. U. (2008) Immediate-early gene regulation by interplay between different post-translational modifications on human histone H3. *J. Cell. Biochem.* **103,** 835–851
41. Guixe, V., Preller, A., Kessi, E., Hofer, H. W., and Ureta, T. (1994) Glycolysis is operative in amphibian oocytes. *FEBS Lett.* **343,** 219–222
42. Dworkin, M. B., and Dworkin-Rastl, E. (1989) Metabolic regulation during early frog development: glycogenic flux in *Xenopus* oocytes, eggs, and embryos. *Dev. Biol.* **132,** 512–523
43. Dworkin, M. B., and Dworkin-Rastl, E. (1991) Carbon metabolism in early amphibian embryos. *Trends Biochem. Sci.* **16,** 229–234
44. Radomski, N., Barreto, G., Kaufmann, C., Yokoska, J., Mizumoto, K., and Dreyer, C. (2002) Interaction of S-adenosylhomocysteine hydrolase of *Xenopus* laevis with mRNA(guanine-7-)methyltransferase: implication on its nuclear compartmentalisation and on cap methylation of hnRNA. *Biochim. Biophys. Acta* **1590,** 93–102
45. Guinez, C., Morelle, W., Michalski, J. C., and Lefebvre, T. (2004) *O*-GlcNAc glycosylation: a signal for the nuclear transport of cytosolic proteins? *Int. J. Biochem. Cell Biol.* **37,** 765–774
46. Datta, B., Ray, M. K., Chakrabarti, D., Wylie, D. E., and Gupta, N. K. (1989) Glycosylation of eukaryotic peptide chain initiation factor 2 (eIF-2)-asso-

ciated 67-kDa polypeptide (p67) and its possible role in the inhibition of eIF-2 kinase-catalyzed phosphorylation of the eIF-2 $\alpha$-subunit. *J. Biol. Chem.* **264,** 20620–20624
47. Roos, M. D., Su, K., Baker, J. R., and Kudlow, J. E. (1997) *O*-Glycosylation of an Sp1-derived peptide blocks known Sp1 protein interactions. *Mol. Cell. Biol.* **17,** 6472–6480
48. Hiromura, M., Choi, C. H., Sabourin, N. A., Jones, H., Bachvarov, D., and Usheva, A. (2003) YY1 is regulated by *O*-linked N-acetylglucosaminylation (*O*-GlcNAcylation). *J. Biol. Chem.* **278,** 14046–14052
49. Gewinner, C., Hart, G., Zachara, N., Cole, R., Beisenherz-Huss, C., and Groner, B. (2004) The coactivator of transcription CREB binding protein interacts preferentially with the glycosylated form of Stat5. *J. Biol. Chem.* **279,** 3563–3572
50. de Moor, C. H., and Richter, J. D. (2001) Translational control in vertebrate development. *Int. Rev. Cytol.* **203,** 567–608
51. Mendez, R., and Richter, J. D. (2001) Translational control by CPEB: a means to the end. *Nat. Rev. Mol. Cell Biol.* **2,** 521–529
52. Maton, G., Lorca, T., Girault, J. A., Ozon, R., and Jessus, C. (2005) Differential regulation of Cdc2 and Aurora-A in Xenopus oocytes: a crucial role of phosphatase 2A. *J. Cell Sci.* **118,** 2485–2494
53. Meikrantz, W., Smith, D. M., Sladicka, M. M., and Schlegel, R. A. (1991) Nuclear localization of an *O*-glycosylated protein phosphotyrosine phosphatase from human cells. *J. Cell Sci.* **98,** 303–307
54. Wells, L., Kreppel, L. K., Comer, F. I., Wadzinski, B. E., and Hart, G. W. (2004) *O*-GlcNAc transferase is in a functional complex with protein phosphatase 1 catalytic subunits. *J. Biol. Chem.* **279,** 38466–38470
55. Cheung, W. D., and Hart, G. W. (2008) AMP-activated protein kinase and p38 MAPK activate *O*-GlcNAcylation of neuronal proteins during glucose deprivation. *J. Biol. Chem.* **283,** 13009–13020
56. Fabian, J. R., Morrison, D. K., and Daar, I. O. (1993) Requirement for Raf and MAP kinase function during the meiotic maturation of Xenopus oocytes. *J. Cell Biol.* **122,** 645–652
57. Uchiyama, K., and Kondo, H. (2005) p97/p47-Mediated biogenesis of Golgi and ER. *J. Biochem.* (*Tokyo*) **137,** 115–119
58. El-Jouni, W., Haun, S., Hodeify, R., Hosein Walker, A., and Machaca, K. (2007) Vesicular traffic at the cell membrane regulates oocyte meiotic arrest. *Development* **134,** 3307–3315
59. Hetzer, M., Meyer, H. H., Walther, T. C., Bilbao-Cortes, D., Warren, G., and Mattaj, I. W. (2001) Distinct AAA-ATPase p97 complexes function in discrete steps of nuclear assembly. *Nat. Cell Biol.* **3,** 1086–1091
60. Wilde, A., Lizarraga, S. B., Zhang, L., Wiese, C., Gliksman, N. R., Walczak, C. E., and Zheng, Y. (2001) Ran stimulates spindle assembly by altering microtubule dynamics and the balance of motor activities. *Nat. Cell Biol.* **3,** 221–227
61. Zhang, C., and Clarke, P. R. (2001) Roles of Ran-GTP and Ran-GDP in precursor vesicle recruitment and fusion during nuclear envelope assembly in a human cell-free system. *Curr. Biol.* **11,** 208–212